doi:10.1006/jmbi.2000.4420 available online at http://www.idealibrary.com on IDEAL® *J. Mol. Biol.* (2001) **306**, 1037–1058

JMB

Structural Origins of Aminoglycoside Specificity for Prokaryotic Ribosomes

Stephen R. Lynch and Joseph D. Puglisi*

Department of Structural Biology, Stanford University School of Medicine, Stanford CA 94305-5126, USA

Aminoglycoside antibiotics, including paromomycin, neomycin and gentamicin, target a region of highly conserved nucleotides in the decoding region aminoacyl-tRNA site (A site) of 16 S rRNA on the 30 S subunit. Change of a single nucleotide, A1408 to G, reduces the affinity of many aminoglycosides for the ribosome; G1408 distinguishes between prokaryotic and eukaryotic ribosomes. The structures of a prokaryotic decoding region A-site oligonucleotide free in solution and bound to the aminoglycosides paromomycin and gentamicin C1a were determined previously. Here, the structure of a eukaryotic decoding region A-site oligonucleotide bound to paromomycin has been determined using NMR spectroscopy and compared to the prokaryotic A-site-paromomycin structure. A conformational change in three adenosine residues of an internal loop, critical for high-affinity antibiotic binding, was observed in the prokaryotic RNA-paromomycin complex in comparison to its free form. This conformational change is not observed in the eukaryotic RNA-paromomycin complex, disrupting the binding pocket for ring I of the antibiotic. The lack of the conformational change supports footprinting and titration calorimetry data that demonstrate approximately 25-50-fold weaker binding of paromomycin to the eukaryotic decoding-site oligonucleotide. Neomycin, which is much less active against *Escherichia coli* ribosomes with an A1408G mutation, binds non-specifically to the oligonucleotide. These results suggest that eukaryotic ribosomal RNA has a shallow binding pocket for aminoglycosides, which accommodates only certain antibiotics.

*Corresponding author

Keywords: eukaryotic; aminoglycoside; 16 S rRNA; paramomycin; NMR

Introduction

Aminoglycosides are a class of antibiotics that bind to the decoding region aminoacyl-tRNA site (A site) of 16 S rRNA (Moazed & Noller, 1987; Woodcock *et al*., 1991), inducing codon misreading and inhibiting translocation (Davies *et al*., 1965; Edelmann & Gallant, 1977). They preferentially target prokaryotic ribosomes over eukaryotic ribosomes, supporting their role as antibiotics. Nonetheless, aminoglycosides inhibit eukaryotic translation at higher concentration (Wilhelm *et al*., 1978a,b).

The aminoglycosides bind to an asymmetric internal loop (U1406-A1408, A1492-U1495) within the decoding region. NMR structural studies on a model oligonucleotide (see the accompanying paper, Lynch & Puglisi, 2001), designed to mimic the minimal binding site of the aminoglycoside antibiotic paromomycin, have shown a conformational change associated with binding of aminoglycoside (Fourmy *et al*., 1996, 1998). The structures of the RNA oligonucleotide in its free form (Fourmy *et al*., 1998), bound to paromomycin (Fourmy *et al*., 1996), and bound to gentamicin C1a (Yoshizawa *et al*., 1998) have been determined. Both aminoglycosides bind in the major groove of the RNA; in both drug-RNA complexes, A1492 and A1493 are displaced towards the minor groove upon binding aminoglycoside (Figure 1). Additionally, A1408 and G1494 shift slightly, so that A1408 and G1494 form a cross-strand stack.

The A1408-A1493 base-pair within the aminoglycoside binding site is critical for high-affinity interaction of antibiotic with RNA (Fourmy *et al*., 1996; Recht *et al*., 1996). This base-pair, along with the displacement of the adenosine residues towards

Abbreviations used: .

E-mail address of the corresponding author: puglisi@stanford.edu

0022-2836/01/051037–22 $35.00/0

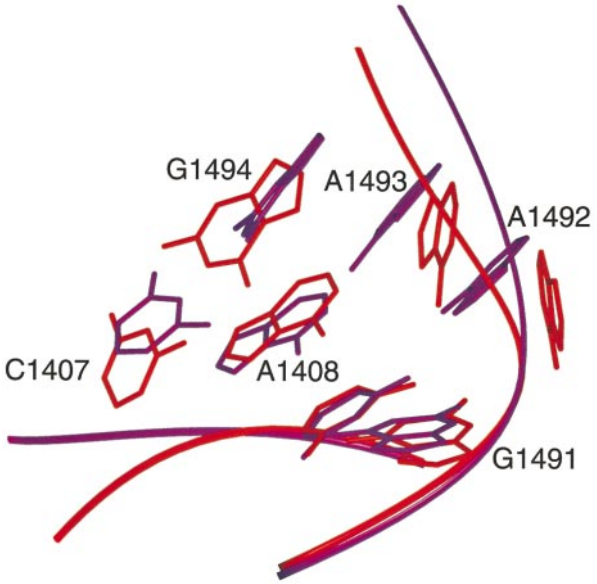

Figure 1. The conformational change in the prokaryotic decoding RNA upon binding paromomycin is shown. The free RNA is shown in purple, the RNA-paromomycin complex is shown in red. The view is towards the major groove of the RNA. Only the bases are shown with a ribbon representing the phosphodiester backbone for simplicity; paromomycin is not shown, it would be coming out of the page with ring I oriented toward A1492 and A1493 and ring II toward G1494 and U1495. A1492 and A1493 change orientation with respect to the helical axis and are displaced toward the minor groove. A1408 stacks under G1494 in the structure of the complex but not in the free-form RNA. The structures of the decoding-site RNA-paromomycin complex (Fourmy *et al*., 1996) and the free-form RNA (Fourmy *et al*., 1998) have been reported.

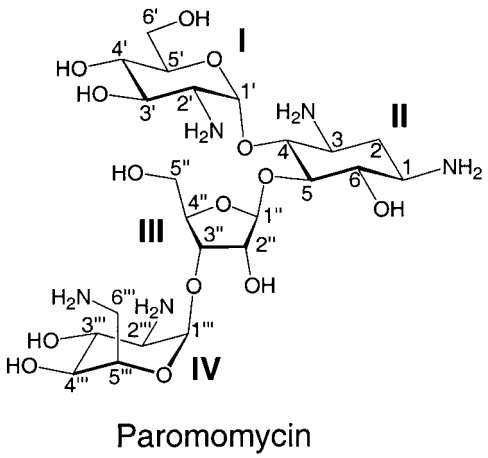

Figure 2. The chemical structure for paromomycin, the four rings and the carbon atoms are labeled by the numbers used in the text. Neomycin is the same except for an amino group on the 6′ position, rather than the hydroxyl group of paromomycin.

the minor groove, creates a pocket for ring I of paromomycin (Figure 2) or gentamicin. The structures of the two RNA-drug complexes are very similar for the RNA internal loop and for rings I and II of the antibiotic, which are common to both drugs; the position of ring III differs, since the linkage of ring III is to a different carbon atom on ring II for gentamicin and paromomycin.

The aminoglycosides target prokaryotic and mitochondrial ribosomes specifically over eukaryotic ribosomes, even though the internal loop contains universally conserved nucleotides at six of the seven positions (Gutell, 1994). The only difference in sequence of the internal loop is at position 1408, which is adenosine in all prokaryotic and mitochondrial sequences, but guanosine in all eukaryotic sequences (Gutell, 1994). Expression of *Escherichia coli* with the mutation A1408G confers high-level (>100-fold) resistance to many aminoglycosides, including neomycin, but only low-level (fourfold) resistance to paromomycin (Recht *et al*., 1999b). Specifically, the single-base mutant conferred resistance to aminoglycosides with a 6′ amino group on ring I, including neomycin, but not those with a 6′ hydroxyl group, including paromomycin. Binding of neomycin to ribosomes with the A1408G mutation was not observed by footprinting (Recht *et al*., 1999a), whereas the affinity of paromomycin binding to ribosomes with the A1408G mutation is decreased approximately 25-50-fold relative to wild-type (Recht *et al*., 1999a). The approximate K_D for paromomycin to *E. coli* ribosomes is 100 nM on the basis of the footprinting data, and approximately 4 mM to ribosomes with an A1408G mutation (Recht *et al*., 1999a). Similarly, footprinting showed no binding of neomycin to the eukaryotic decoding-site oligonucleotide and binding to paromomycin to the eukaryotic oligonucleotide was decreased 25-50-fold. A 40-fold decrease in binding affinity of paromomycin to the eukaryotic oligonucleotide compared to the prokaryotic oligonucleotide was measured by titration calorimetry (R.G. Eason, M. Recht & J.D. P., unpublished results).

Differences in RNA structure between prokaryotic and eukaryotic drug-binding sites are the origin of aminoglycoside specificity for bacteria. The A1408-A1493 base-pair in the prokaryotic structures creates a binding pocket for ring I. The geometry of the A-A pair cannot be replaced by an isosterically duplicated G-A pair, as it would be in the eukaryotic sequence (see Lynch & Puglisi, 2001). The structure of the free-form eukaryotic decoding region A-site oligonucleotide is reported in the accompanying paper (Lynch & Puglisi, 2001), and has minor conformational differences from the prokaryotic RNA oligonucleotide. As expected, the base-pairing between the 1408 position and A1493 differs in the two structures. Only one hydrogen bond was observed between the amino proton of G1408 and N1 of A1493. The G1408-A1493 base-pair was disordered, but the

average geometry was close to a normal G-A imino base-pair. The carbonyl group of G1408 projects into the major groove of the RNA near the binding site for ring I of paromomycin in the prokaryotic RNA-drug complex. A disruption in the ring I binding site supports the biological data, which showed resistance of A1408G ribosomes to aminoglycosides with an amino group on the 6′ position on ring I.

This study is aimed at identifying the structural origins of aminoglycoside specificity for prokaryotic ribosomes by determining the structure of a eukaryotic decoding-site oligonucleotide bound to paromomycin. The structure was determined with homonuclear and heteronuclear NMR experiments and compared to the previous prokaryotic decoding-site RNA-paromomycin (Fourmy *et al*., 1996) and the free eukaryotic decoding-site oligonucleotide structures (Lynch & Puglisi, 2001). The structure of the eukaryotic RNA bound to paromomycin shows no displacement of the adenosine residues upon antibiotic binding, and comparison of the two paromomycin complexes suggests why the A1408G mutation decreases the affinity for paromomycin.

Results

Oligonucleotide design

The decoding-site RNA oligonucleotide used in this study is presented in the accompanying paper (Lynch & Puglisi, 2001). This oligonucleotide represents the simplest model eukaryotic decoding region A-site oligonucleotide and can be used to identify the specificity of aminoglycosides for prokaryotic ribosomes. This oligonucleotide is a valid model system for NMR study of aminoglycoside rRNA interaction (Recht *et al*., 1996).

NMR assignments of the eukaryotic decoding-site oligonucleotide bound to paromomycin

Paromomycin forms a 1:1 complex with the eukaryotic decoding-site oligonucleotide. The quality of the NMR spectra of the eukaryotic oligonucleotide bound to paromomycin was good, although resonances were broader than those of the free RNA. A titration of paromomycin into the RNA is presented in Figure 3. The resonances for U1490 and G1491 shift downfield upon addition of drug. The RNA-paromomycin complex is in slow exchange on the NMR time-scale, as shown by the two resonances for U1490 and G1491 at a 0.5:1 stoichiometry of drug to RNA. Slight changes in chemical shift are observed for the imino resonances of U1406, G1494 and U1495.

Chemical shift is a very sensitive indicator of change in local chemical environment surrounding a proton. Comparison of assignments of the two oligonucleotides bound to paromomycin is shown in Table 1 for the base and H1′ protons for the core nucleotides (G1405-A1410, U1490-C1496). More resonances are affected by drug binding to the prokaryotic oligonucleotide than by drug binding to eukaryotic oligonucleotide. Additionally, changes in excess of 0.5 ppm are observed for the aromatic protons on A1408 and the imino proton on G1491 in the prokaryotic complex, whereas the largest change for any proton of the eukaryotic RNA was 0.15 ppm for the G1491 imino resonance.

The chemical shift differences suggest a greater RNA conformational change upon drug binding to prokaryotic RNA than to eukaryotic RNA. Large conformational changes occur in the prokaryotic RNA upon paromomycin binding; A1492 and A1493 are displaced toward the minor groove, and change orientation with respect to the helix (Figure 1). With the small chemical shift differences observed in the eukaryotic RNA, a major change in A1492 and A1493 would not be expected.

Table 1. Comparison of NMR chemical shifts of paromomycin-bound prokaryotic and eukaryotic oligonucleotides

	H8/6		H5/2		H1′		Imino	
	G1408	A1408	G1408	A1408	G1408	A1408	G1408	A1408
G1405	7.47	**7.58**	-	-	5.75	5.81	13.27	13.22
U1406	7.58	**7.34**	5.17	**5.32**	5.46	5.49	10.66	**11.1**
C1407	7.98	**7.8**	5.71	5.73	5.72	5.65	-	-
A/G1408	7.69	**7.85**	-	**6.92**	5.82	5.97	(13.21)	-
C1409	7.68	7.46	5.43	5.43	5.46	**5.12**	-	-
A1410	8.19	8.07	7.43	7.55	5.91	**5.98**	-	-
U1490	**7.74**	7.68	5.13	5.18	5.53	5.56	**14.07**	**14.39**
G1491	7.70	**7.84**	-	-	5.70	**5.96**	**12.38**	**13.06**
A1492	**8.22**	**8.22**	7.75	7.95	6.05	5.96	-	-
A1493	8.41	8.21	**8.21**	**8.22**	6.12	6.06	-	-
G1494	7.71	**7.55**	-	-	5.72	**5.82**	13.14	**12.64**
U1495	7.61	**7.77**	5.21	5.25	5.49	5.53	**10.35**	10.33
C1496	8.09	8.1	5.85	5.76	5.75	5.76	-	-

[1]H chemical shift was measured at 35 °C for non-exchangeable protons; 5 °C for exchangeable protons. The sample was ~3 mM RNA in 10 mM sodium phosphate (pH 6.3).

Resonances that shifted by >0.1 ppm upon binding of paromomycin are indicated in bold.

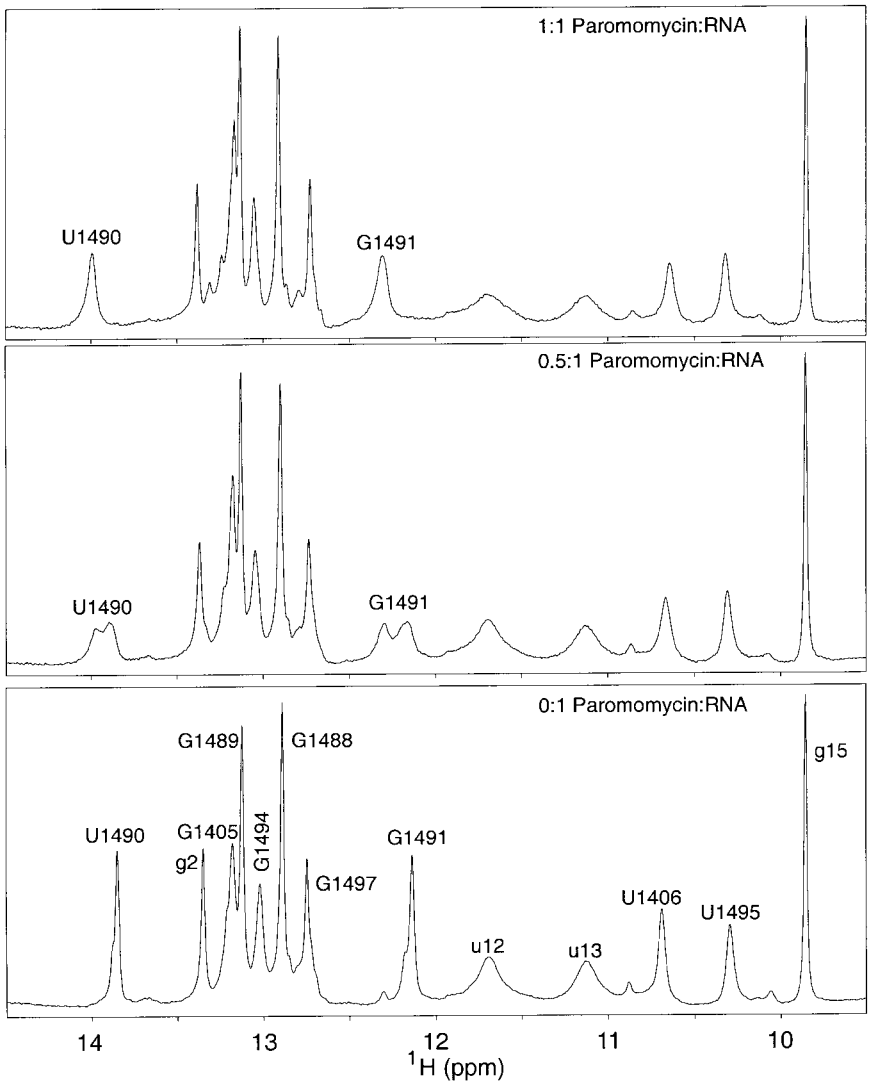

Figure 3. The 1D NMR spectrum of a titration of paromomycin into the eukaryotic decoding-site oligonucleotide. The lower panel is the free RNA, the middle panel is a 0.5:1 complex of drug/RNA, and the top panel is a 1:1 complex. The titration was performed on a sample of 3 mM RNA at 25 °C on a Varian Inova 500 MHz spectrometer. The downfield portion of the spectrum, which includes the guanosine and uridine imino proton resonances, is shown.

NMR characteristics of the eukaryotic oligonucleotide bound to paromomycin

All non-exchangeable protons and most exchangeable protons were assigned for the eukaryotic oligonucleotide in the 1:1 paromomycin complex through homonuclear and heteronuclear (^{1}H, ^{13}C, ^{15}N, ^{31}P) 2D, 3D and 4D experiments.

The imino resonance for G1408 was tentatively assigned. The resonance appears as a weak, broad shoulder on the G1489 imino in a 1D spectrum and a ^{1}H-^{15}N HSQC. A potential NOE to the G1491 imino proton was very weak and observed only at long mixing time at 25 °C on the 800 MHz spectrometer. The G1408 imino proton is presumed to be broad due to solvent exchange and the conformational dynamics of the weaker-affinity eukaryotic RNA-paromomycin complex. Additionally, all of the imino protons in the vicinity of the internal loop (G1405, U1406, G1491, G1494 and U1495) were broader than in the free form, indicating intermediate exchange dynamics of the RNA-paromomycin complex.

Strong H1′/H2′ crosspeaks were detected in the (^{1}H/^{1}H) DQF-COSY and short mixing time (20 ms) (^{1}H/^{1}H) TOCSY for A1492 and A1493 as well as u13 and c14 of the UUCG tetraloop. In addition, very weak H1′/H2′ crosspeaks were detected in the (^{1}H/^{1}H) DQF-COSY or short mixing time (20 ms) (^{1}H/^{1}H) TOCSY for G1491 and G1408, in addition to g1 and c27. Weak H1′/H2′ crosspeaks in the TOCSY and DQF-COSY indicate mixed sugar puckers or dynamics for these residues.

For paromomycin in the RNA-drug complex, crosspeaks for ring I H1′/H2′, ring III H1″/H2″, and ring IV H1‴/H2‴ were observed in the DQF-COSY. The coupling constants measured are in agreement with the chair conformations observed

for rings I and IV in the prokaryotic complex, but the strong ring III H1″/H2″ crosspeak indicates a C2′-*endo* sugar pucker for the ribose ring. No crosspeak was observed for ring III for the prokaryotic complex, indicating a C3′-*endo* sugar pucker.

The canonical set of *A*-form intranucleotide and internucleotide NOEs, including those from the H1′, H2′, and H3′ protons to the intranucleotide H8/6 protons and the H8/6 protons of the sequential nucleotide, with comparatively similar intensities, were observed from g1 through C1412, including the C1407 to G1408 and G1408 to C1409 steps. The canonical *A*-form NOEs were not observed on the other side of the internal loop, particularly the G1491-A1492, A1492-A1493, and A1493-G1494 steps, which was observed also in the spectra of the free-form eukaryotic RNA. However, no NOE was detected from G1491 to A1493, indicating that A1492 is not bulged out of the helix.

The relative intensities of NOEs in the *A*-form region (g1-G1405, C1409-C1412, G1488-G1491) were basically the same in the free and bound RNA. The UUCG tetraloop has the same unusual NMR characteristics as in the free form and other RNA sequences. The NOEs in the internal loop were very similar, except for slight changes in NOEs involving the aromatic protons, particularly those of A1492 and A1493.

The NOE patterns involving A1492 and A1493 are different in the eukaryotic RNA-paromomycin complex (Figure 4) compared to prokaryotic RNA-aminoglycoside complexes. In the prokaryotic RNA-paromomycin and gentamicin complexes, the A1493 (H2)-C1409 (H1′) NOE was observed, but was weak in intensity; an NOE from A1493 (H2) to the G1494 (H1′) was not observed, and these two protons are approximately 7.5 Å apart in the structure. In the eukaryotic RNA-paromomycin complex, the A1493 (H2)-C1409 (H1′) NOE is observed at short mixing time (50 ms) (Figure 4(a)) and is moderate in intensity, weaker than the strong intranucleotide H5-H6 NOEs. The ^{13}C-edited NOESY (Figure 4(b)) confirms the assignment of this NOE to the A1493 (H2) rather than the A1492 (H8). The A1493 (H2)-G1494 (H1′) NOE is observed at 150 ms in both 2D and 3D NOESY experiments, and is readily identified in the 3D NOESY experiments. These two NOEs demonstrate that the conformation of the base of A1493 relative to G1494 and C1409 must be different in the prokaryotic oligonucleotide-paromomycin complex in comparison to the eukaryotic oligonucleotide-paromomycin complex. This result is important, because A1493 in the prokaryotic RNA changed conformation upon binding paromomycin and gentamicin C1a.

Structure of eukaryotic oligonucleotide bound to paromomycin

The structure of the eukaryotic A-site oligonucleotide-paromomycin complex was calculated from 605 RNA-RNA NOEs, 13 paromomycin-paromomycin NOEs (all inter-ring), 37 RNA-paromomycin NOEs, 122 experimentally determined RNA-RNA dihedral constraints, 35 paromomycin-paromomycin dihedral constraints and 36 hydrogen bonds for the Watson-Crick base-pairs. In all, 100 structures were calculated, of which 35 converged to low energy after the global fold; the NOE and dihedral violation energies for seven structures were high after refinement with torsion angle restraints and thus were discounted. Structure statistics for the eukaryotic oligonucleotide-paromomycin complex are presented in Table 2.

A comparison of intermolecular NOEs in the eukaryotic and prokaryotic complexes is presented in Table 3. The total number of assigned intermolecular NOEs is less in the eukaryotic complex, in particular those involving ring I. The lack of NOEs to ring I is consistent with a disruption in the ring I binding pocket, which was formed by the A1408-A1493 base-pair in the prokaryotic complex, and a different G1408-A1493 base-pair in the eukaryotic complex. Additionally, the NOEs for ring I are to the aromatic protons of A1492 in the eukaryotic RNA rather than the sugar protons, also suggesting a different binding pocket for ring I.

A superposition of the 28 lowest-energy structures of the eukaryotic oligonucleotide-paromomycin complex is presented in Figure 5(a). The overall r.m.s.d. for the RNA is 1.17 Å. The overall r.m.s.d. is lower than in the free-form oligonucleotide (1.50 Å) because the drug acts as an axis that connects the lower and upper stems. Figure 5(b) presents the superposition of only the core residues (G1405-A1410, U1490-C1496) with paromomycin; the r.m.s.d. of these residues to a minimized average is 0.86 Å. The disorder of these residues is primarily from the positions of ring I and IV to the RNA.

The positions of the bases and much of the RNA backbone and paromomycin rings II and III are well defined when superimposing only the core residues and paromomycin. In the prokaryotic RNA-paromomycin complex, rings I and II were well defined, while rings III and especially IV were not. The lack of NOEs to ring I from the eukaryotic RNA accounts for the difference in disorder. The relative disorder of ring II in the eukaryotic complex compared to the prokaryotic complex results primarily from transmission of the disorder of the position of ring I to the RNA.

The structure of paromomycin is well defined by the intramolecular NOEs and paromomycin torsion angle constraints as shown in Figure 5(c). Rings I and II adopt the same conformations as in the prokaryotic complex. Ring III adopts a C2′-*endo* conformation in the eukaryotic complex, as opposed to the C3′-*endo* conformation observed in the prokaryotic complex. Ring IV remains disordered, as in the prokaryotic complex.

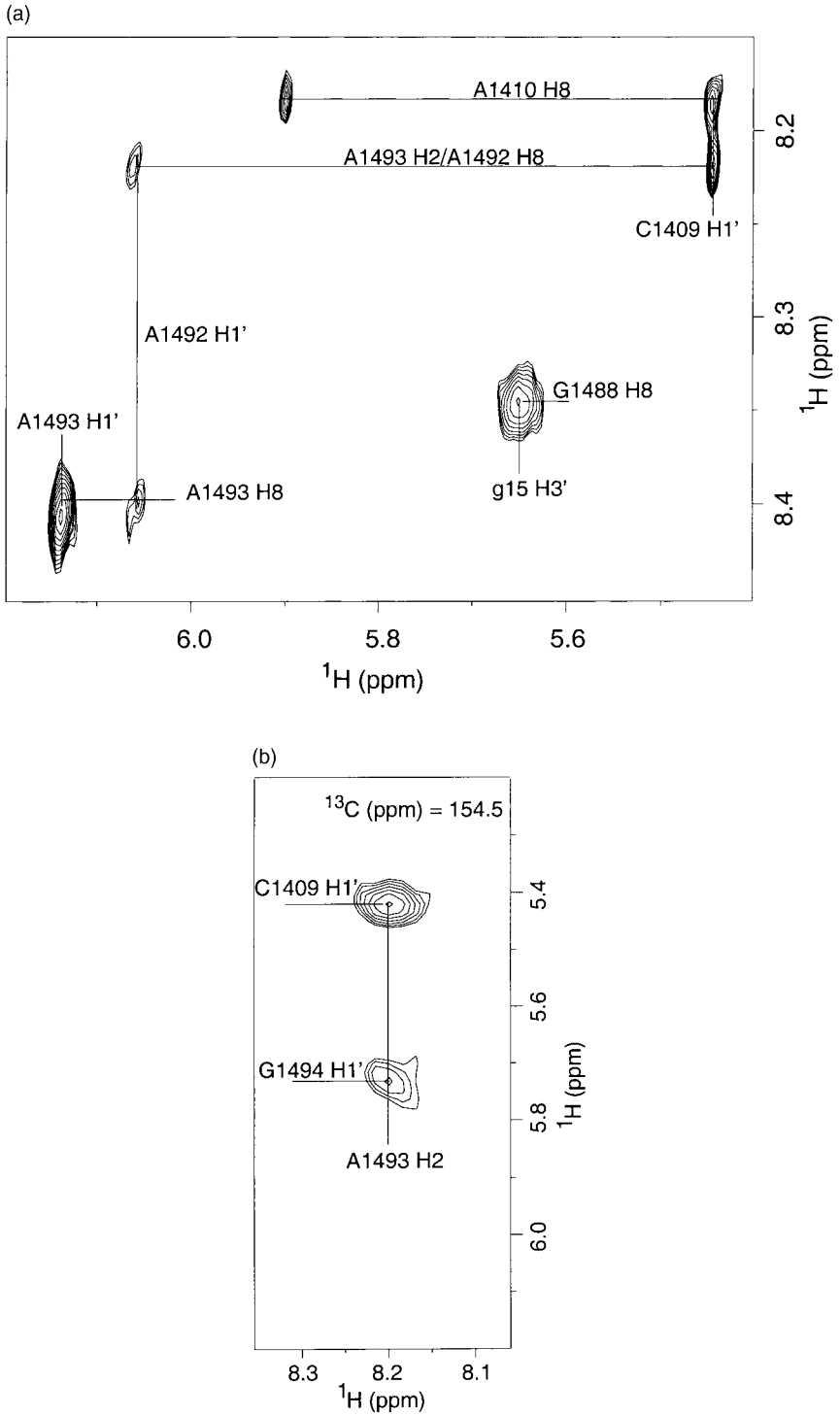

Figure 4. (a) A portion of a 2D (^{1}H/^{1}H) NOESY experiment acquired at 35 °C with a 50 ms mixing time on a 1:1 eukaryotic RNA/paromomycin complex. The spectrum was acquired in 24 hours on a sample of 3 mM RNA at 500 MHz with 64 scans of 2048 complex points in ω2 by 512 in ω1. The portion of the spectrum shown is a section of the H1′/base crosspeaks. The most important NOE is from a resonance at 8.22 ppm to the H1′ of C1409. This NOE could be from either A1493 H2 or A1492 H8. (b) A portion of a plane of a 3D NOESY-HSQC (^{1}H/^{13}C/^{1}H) acquired at 35 °C with a mixing time of 150 ms on a 2 mM, fully ^{13}C,^{15}N-labeled, eukaryotic decoding-site RNA oligonucleotide bound to paromomycin in ^2H_2O on a Varian Inova 500 MHz spectrometer is shown. The spectrum was acquired in 70 hours with eight scans of 2048 complex points in ω3 by 64 in ω2 (^{13}C) by 128 in ω1 (^{1}H). A ^{13}C plane at 154.5 ppm is shown; this carbon shift corresponds to C2 of A1493. The NOE shown in (a) that could not be distinguished between A1492 H8 and A1493 H2 is demonstrated to be from A1493 H2. An additional NOE, to the H1′ of G1494 is observed at the longer mixing time.

Table 2. Structure statistics and atomic r.m.s. deviations

Distance constraints	
Total	655
Internucleotide (RNA-RNA)	380
Internal loop (RNA-RNA)	164
Internucleotide internal loop	105
RNA-paromomycin	37
Paromomycin-paromomycin	13
Dihedral constraints	
RNA	122
Paromomycin	35
Hydrogen bonds (WC base-pairs)	36
Final forcing energies (kcal/mol)	
Distance and dihedral constraints	5.76 ± 0.87
r.m.s.d from distance constraints (Å)	
All (655)	0.00687
r.m.s.d. from experimental dihedral constraints (deg.) (122)	0.525
Deviations from idealized geometry	
Bonds (Å)	0.152
Angles (deg.)	8.26
Impropers (deg.)	0.734
Heavy-atom r.m.s.d	
All RNA	1.17
Paromomycin	0.93
Core residues + paromomycin	0.86
Core residues − paromomycin	0.78
Core residues + ring I	0.84
Core residues + ring II	0.78
Core residues + ring III	0.82
Core residues + ring IV	0.90

Final minimized structures are compared to the average coordinates of the 28 final structures best-fitted to each other. The final structures did not contain any NOE violations >0.2 Å or torsion angle violations > 10°. Core residues refer to G1405-A1410 and U1490-C1496. Internal loop residues refer to U1406-G1408 and A1492-U1495. WC base-pairs are Watson-Crick G-C and A-U base-pairs.

Comparison of the structures for the eukaryotic and prokaryotic decoding-site RNA bound to paromomycin

The paromomycin complexes of the prokaryotic and eukaryotic decoding-site oligonucleotides are presented in Figure 6. The structure of the prokaryotic oligonucleotide-paromomycin complex was determined previously, and is shown here for comparison. The global structure of the two oligonucleotides is similar; the upper stem, lower stem, and UUCG tetraloop are equivalent, as expected. The overall r.m.s.d between the structures of the prokaryotic and eukaryotic decoding-site oligonucleotides bound to paromomycin is 3.99 Å; the r.m.s.d. for the internal loop and paromomycin of the two structures is 4.32 Å and for the internal loop without paromomycin is 4.07 Å.

Paromomycin binds in the major groove of the RNA in both structures. Ring I is positioned near the adenosine stack of A1492 and A1493. Ring II is near the U1406-U1495 base-pair. Ring III points down from ring II towards the lower stem, and ring IV is in position to contact the phosphodiester backbone. In the prokaryotic RNA-drug complex, ring I is buried in the RNA-drug complex, whereas ring I is more exposed to solvent in the eukaryotic RNA-drug complex. The difference in the binding pocket for ring I affects all four rings of paromomycin.

The RNA structures in the two complexes are globally similar. U1406 base-pairs to U1495, C1407 base-pairs to G1494 in a Watson-Crick geometry, and the 1408 position to A1493. In the eukaryotic RNA U·U pair, the U1406 imino hydrogen atom bonds to the U1495 O4 (3.61(±0.20) Å) rather than the U1495 O2 (6.38(±0.60) Å), and the U1495 imino proton is closer to U1406 O2 (4.88(±0.37) Å) than it is to U1406 O4 (5.42(±0.92) Å). The one

Table 3. Comparison of intermolecular NOEs for prokaryotic RNA-paromomycin complex and eukaryotic RNA-paromomycin complex

	Prokaryotic RNA/ paromomycin	Eukaryotic RNA/ paromomycin
Total	47	37
RNA-ring I	13	7
RNA-ring II	19	11
RNA-ring III	5	5
RNA-ring IV	10	14
Drug-G1405	0	1
Drug-U1406	4	4
Drug-C1407	4	4
Drug-A/G1408	2	0
Drug-G1489	1	0
Drug-U1490	8	11
Drug-G1491	5	1
Drug-A1492	5	3
Drug-A1493	7	3
Drug-G1494	5	3
Drug-U1495	6	7

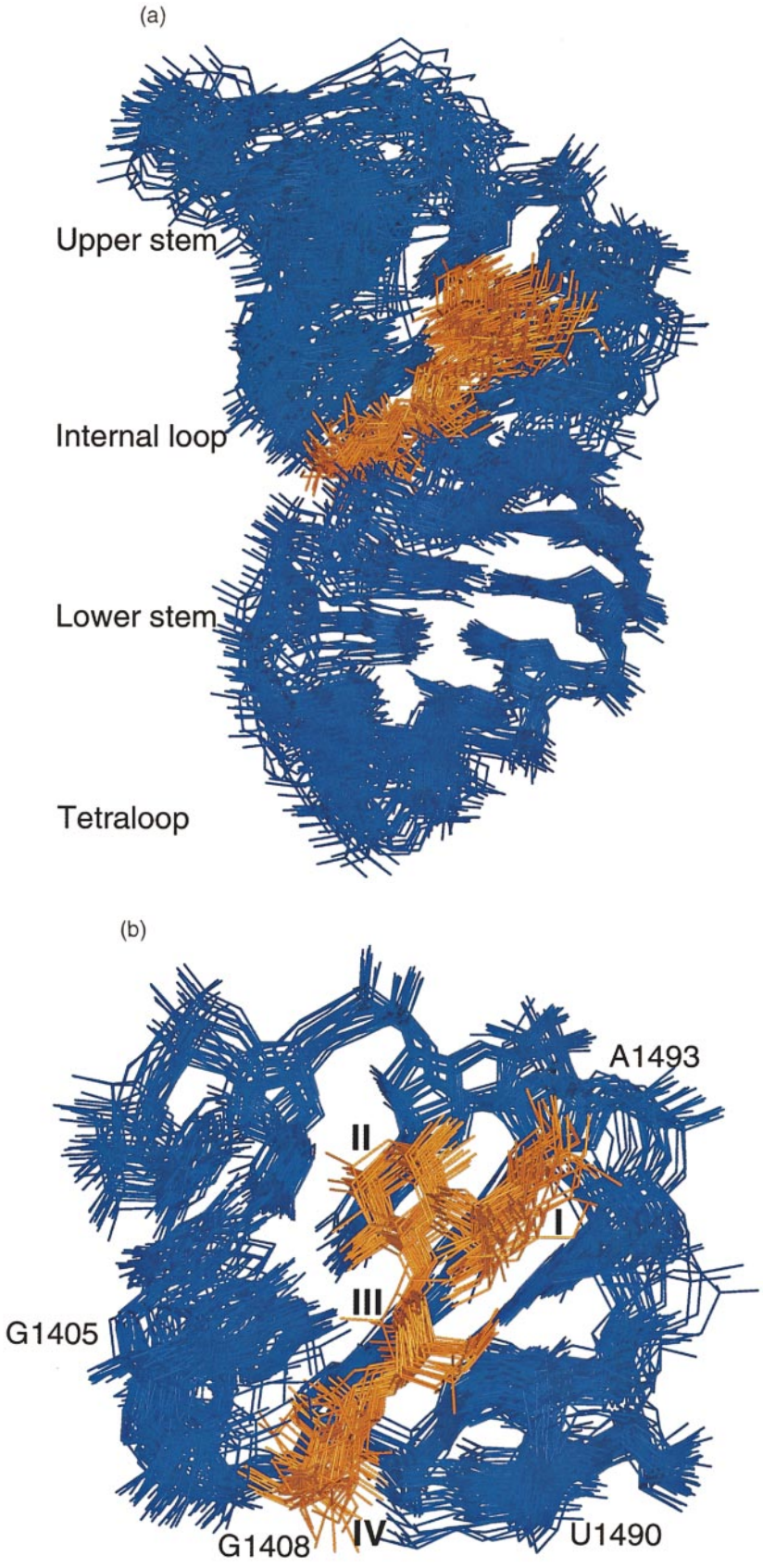

Figure 5(a) and (b) (*legend opposite*)

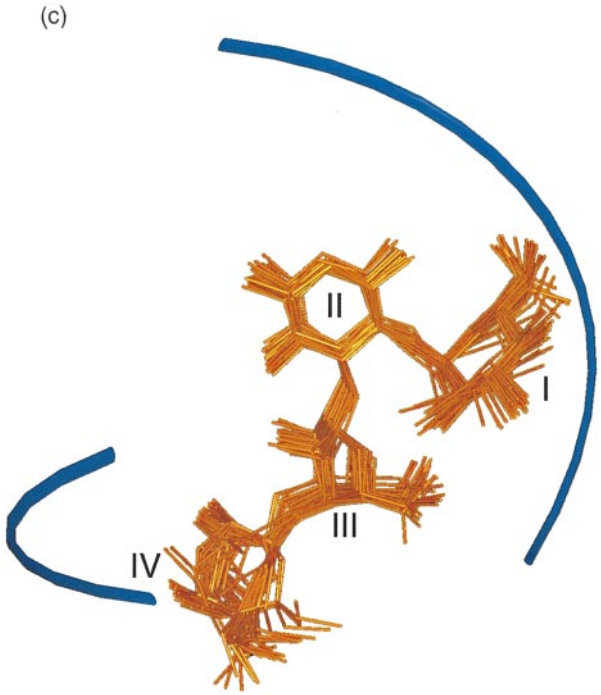

Figure 5. (a) Superposition of the 28 lowest-energy structures of the eukaryotic decoding-site oligonucleotide; the r.m.s.d. of these structures to the average was 1.17 Å. The RNA is blue, the paromomycin is gold. Paromomycin binds in the major groove of the RNA. (b) Superposition of the 28 lowest-energy structures of the core residues (G1405-A1410, U1490-C1496) and paromomycin of the eukaryotic decoding-site oligonucleotide/paromomycin complex; the r.m.s.d. of these structures to the average was 0.86 Å. (c) The superposition of the 28 lowest-energy structures of paromomycin of the eukaryotic decoding-site oligonucleotide/paromomycin complex. The four rings of paromomycin are labeled. Rings II and III are well defined, rings I and IV are not as well defined.

potential geometry on the U-U base-pair is favored over the other, but the donor and acceptor atoms are not close in space. The long distances between the hydrogen bond donors and acceptors is an indication of possible water-mediated hydrogen bonds. The imino protons for both U1406 and U1495 are observed and a strong-intensity NOE is observed between the U1406 and U1495 imino protons, but the resonances are broader than in the free form, and the number of NOEs assigned for each imino proton was less than in the free form.

The structure of the prokaryotic RNA-paromomycin complex shows the two imino protons facing each other; the distance from the U1406 N3 does not favor interaction with either carbonyl group of U1495 (4.46(±0.14) Å, U1406 N3-U1495 O4; 4.59(±0.38) Å U1406, N3-U1495 O2). The U1495 N3 favors interaction with the U1406 O4 (3.95(±0.40) Å) over the U1406 O2 (5.37(±0.13) Å) in the prokaryotic RNA-paromomycin complex. The U1406 and U1495 imino protons could be assigned from each other through correlation experiments developed since the publication of the structure of the prokaryotic complex (Simorre *et al*., 1995); thus the somewhat different NOEs observed could be distinguished from each other in this study. The orientation of U1406 to U1495 was not affected by the binding of paromomycin in either case.

The G1408-A1493 base-pair is better defined in the paromomycin complex than in the free form, which is similar to the finding that the A1408-A1493 base-pair is better defined in the prokaryotic RNA-paromomycin complex than in the free form. In the eukaryotic oligonucleotide, two amino protons were observed for A1493 but only one for A1492, as expected. The G1408 imino resonance was tentatively assigned on the basis of the 1D imino spectra, 2D ($^{15}N/^{1}H$) HSQC, and 2D ($^{1}H/^{1}H$) NOESY data, but the putative imino proton could never be correlated to the aromatic proton of G1408, and there were not enough NOEs to confidently assign the imino proton. The amino protons for G1408 were not observed.

A moderately intense A1493 H2-C1409 H1′ NOE (Figure 4) positions the Watson-Crick face of A1493 toward G1408; C1407 ribose to G1408 H8 NOEs, G1408 ribose to C1409 H5 and H6 NOEs, and a G1494 imino proton to G1408 H1′ position the Watson-Crick face of G1408 toward A1493 (Figure 7). The structures show a normal G-A imino base-pair with hydrogen bonds between the imino proton of G1408 and N1 of A1493 (N-N distance 2.86(±0.20) Å), and the amino protons of A1493 and the O6 carbonyl of G1408 (N-O distance 3.27(±0.40) Å) (Figure 7). The other common G-A base-pair is the sheared G-A, which involves the adenosine amino group hydrogen bonding to the guanosine N3 and the guanosine amino group hydrogen bonding to the adenosine N7. The sheared G-A geometry is not supported by the NMR data.

The position of the internal loop nucleotides relative to the lower stem for the two structures is quite different (Figure 8). The bases of the A1492 and A1493 are not displaced toward the minor groove and not oriented nearly perpendicular to the helical axis in the structure of the eukaryotic

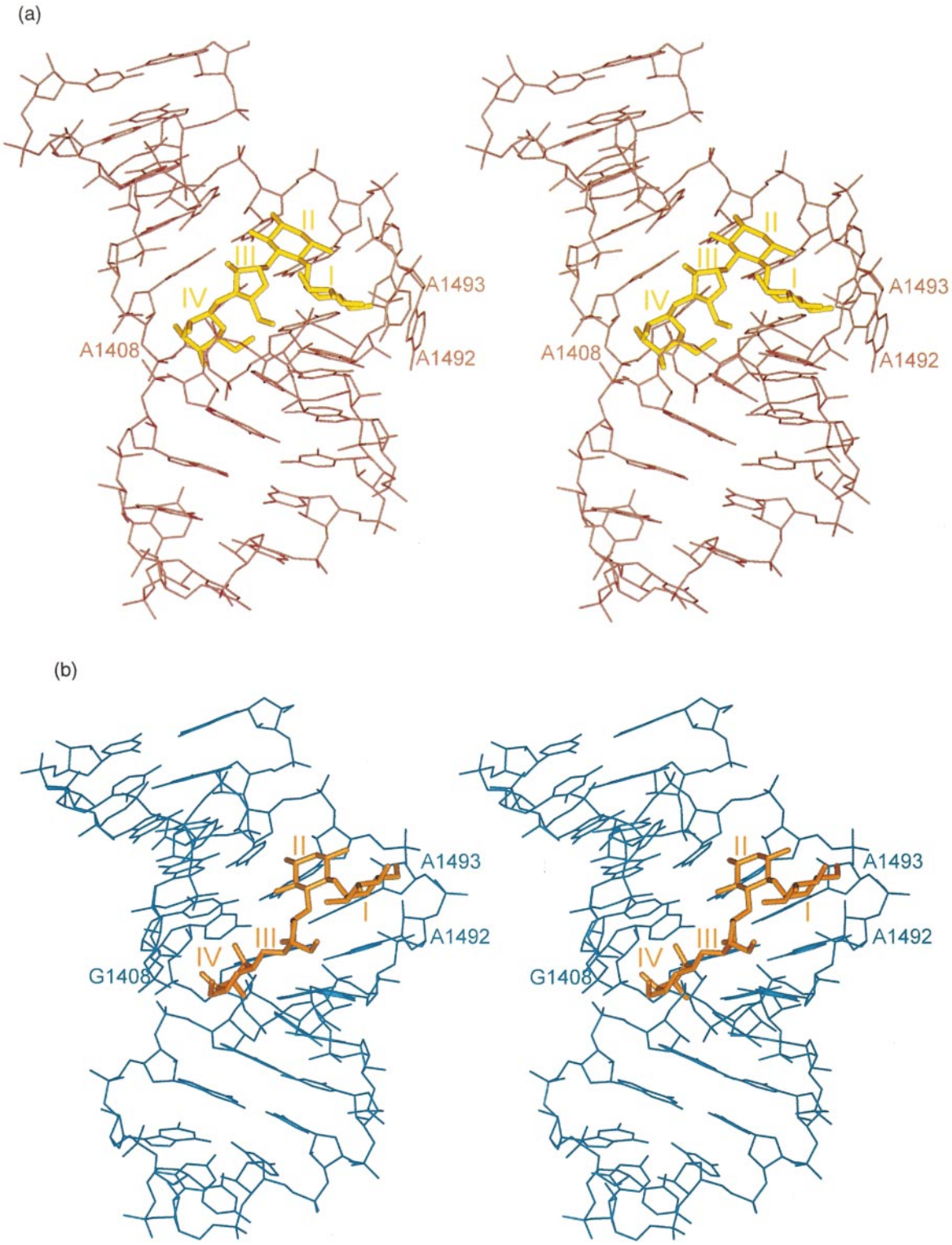

Figure 6. A comparison (stereo) of the median-energy structure of the eukaryotic decoding-site oligonucleotide (blue) and prokaryotic decoding-site oligonucleotide (red), each bound to paromomycin (gold). The structure of the prokaryotic RNA/drug complex has been determined (Fourmy *et al.*, 1996).

oligonucleotide-paromomycin complex, in contrast to that of the prokaryotic RNA complex. In the prokaryotic structure, A1408 stacks underneath G1494, and forms a base-pair with A1493, shifting A1493 and A1492 to the minor groove relative to the helical axis. In the eukaryotic RNA-paromomycin complex, A1493 rather than G1408 stacks under G1494, and A1492 stacks under A1493. G1408 stacks between C1407 and C1409. The different position of G1408, A1492 and A1493 clearly

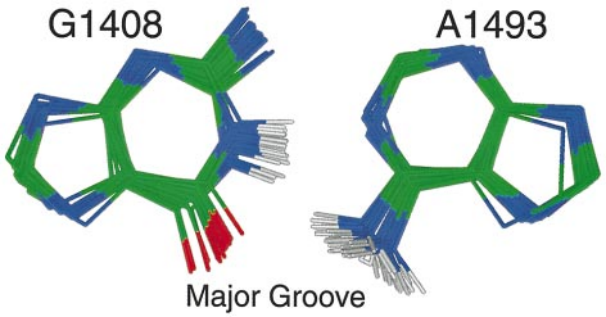

Figure 7. Superposition of the 28 lowest-energy structures of G1408 and A1493 in the eukaryotic RNA/paromomycin complex structure. The structures converge to a normal G-A imino base-pair with hydrogen bonds from the G1408 imino proton to A1493 N1 and the A1493 amino protons to the G1408 O6 carbonyl group. The view is from the C1407-G1494 base-pair down at the G-A base-pair. The position of ring I of paromomycin is shown as a circle. The position of the major groove is indicated.

perturbs the binding pocket for ring I in the eukaryotic complex compared to the prokaryotic complex.

Figure 9 highlights the difference in the positions of both the 1408 nucleotide and A1493. In the eukaryotic complex, A1493 is not displaced or rotated so that the adenosine 6-amino group rather than N7 is pointed into the major groove. The G1408 O6 carbonyl group also protrudes into the major groove. The bulky functional groups force ring I to be in a different conformation relative to the RNA (Figure 8(b)) in the two structures, which is then transmitted to the other rings of paromomycin.

The G1408-A1493 base-pair disrupts the binding site for ring I (Figure 10). In the prokaryotic RNA-paromomycin complex, the displacement of A1492 and A1493 creates space for ring I to stack on the base of G1491. Ring I is buried in the surface of RNA, makes specific contacts from the 6′ hydroxyl (mean C6′-O distance 4.50(±0.48) Å) and 4′ hydroxyl groups (mean O-O distance 3.74(±0.24) Å) to the phosphate oxygen atom of A1493 and the 3′ hydroxyl group to the phosphate oxygen atom of A1492 (mean O-O distance 3.94(±1.11) Å). In the eukaryotic RNA-paromomycin complex, ring I is not buried in the RNA; the RNA surface prevents ring I from fully engaging with its binding site. Ring I is not stacked on G1491 as in the prokaryotic complex. Similar contacts are made to the backbone surrounding A1492 and A1493: the ring I 3′ hydroxyl group is close to the phosphate oxygen atom of A1492 (mean O-O distance of 4.10(±0.77) Å, median O-O distance 3.84 Å) in the ensemble of structures, and the ring I 6′ hydroxyl group is close to the phosphate oxygen atom of A1493 (mean O-O distance of 3.32(±0.52) Å, median O-O distance 3.14 Å). The ring I 4′ hydroxyl group is not very close to a phosphate oxygen atom of either A1492 or A1493 (mean 4′ OH-A1492 phosphate oxygen O-O distance 4.62(±0.60) Å; mean 4′ OH-A1493 phosphate oxygen O-O distance 5.93(±0.41) Å). The dynamic nature of ring I, caused by disruption of its binding site by the G1408-A1493 pair, prevents formation of the stable contacts to the phosphodiester backbone that are observed in the prokaryotic complex (Fourmy *et al.*, 1996).

Structure of paromomycin in the eukaryotic and prokaryotic RNA-drug complexes

Paromomycin adopts globally similar structures in both prokaryotic and eukaryotic complexes (Figure 11). Rings I and II are in the same conformation in both structures. Both rings adopt a chair conformation with the bulky substituents, the amino groups and hydroxyl groups, in the equatorial positions. The two rings are also oriented nearly identically with respect to each other in both complexes. Ring III adopts a C2′-*endo* conformation in the eukaryotic complex in contrast to the C3′-*endo* conformation in the prokaryotic complex. Ring IV is disordered, but is in a chair conformation in all low-energy structures for the eukaryotic complex.

The difference in the structure of paromomycin between the two complexes results primarily from the difference in sugar pucker of ring III. This structural change causes a change in position of ring IV relative to ring III. The difference in sugar pucker allows rings III and IV to make more contacts to the RNA. Position G1408 causes the difference in rings III and IV indirectly because of a change in the binding pocket for ring I, which will be discussed later.

Contacts made by paromomycin to the eukaryotic decoding-site oligonucleotide

Paromomycin forms intramolecular and intermolecular hydrogen bonds in the eukaryotic RNA-paromomycin complex (Figure 12). Since none of the exchangeable protons was assigned for the drug, the positions for the hydrogen bond donors to the RNA depend upon NOEs from non-exchangeable protons. The distances between heavy atoms are summarized in Table 4. The hydrogen bonds shown in Figure 12 include the ring III 2″ hydroxyl group to the O6 carbonyl group of G1408, the ring II 6 hydroxyl group to the O4 carbonyl group of U1406, and a bifurcated hydrogen bond from the ring II 1 amino group to N7 of G1494, and the O4 carbonyl group of U1495.

Ring II of paromomycin directs sequence-specific RNA recognition in the eukaryotic RNA complex, similar to its role in the prokaryotic RNA-paromomycin complex. Three base-specific contacts were observed to ring II, the 6 hydroxyl group to the O4 carbonyl group of U1406, the 1 amino group to G1494 N7 and the O4 carbonyl group of U1495.

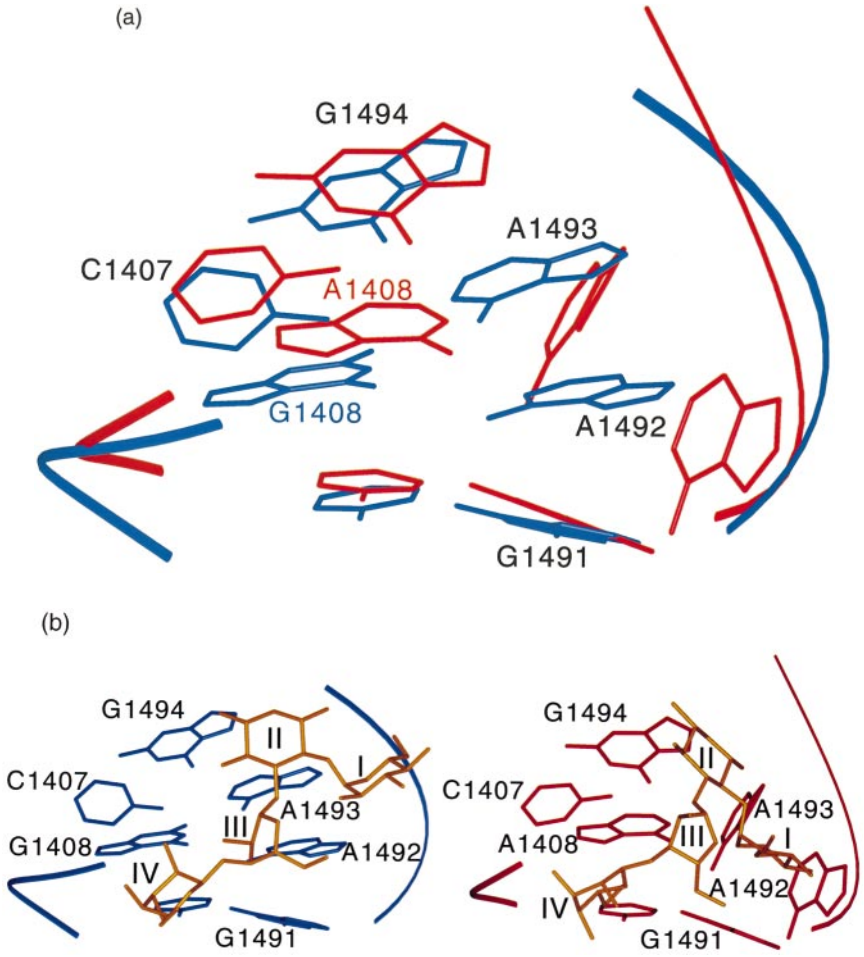

Figure 8. (a) The lower stem residues (C1409-C1411; G1489-G1491) of the eukaryotic RNA/paromomycin complex (blue) were superimposed on the same nucleotides of the prokaryotic RNA/paromomycin complex (red). The view in the Figure is toward the major groove of the internal loop. The ribbons represent the phosphodiester backbone. This Figure highlights the differences between the two complexes in position and orientation of A1492 and A1493, and of C1407, G1408, and G1494 in the internal loop relative to the lower stem. Paromomycin is not shown to better show the differences in conformation of the RNA; paromomycin would be coming out of the page. (b) The same view of the two structures, now side-by-side rather than superimposed, to show where paromomycin (gold) is with respect to the RNA.

The distortion of the ring I binding pocket by the G1408-A1493 base-pair *versus* the A1408-A1493 base-pair in the prokaryotic sequence causes ring II to orient somewhat differently relative to the RNA, particularly to the U1406-U1495 base-pair. The 1 amino group makes the same contact to U1495, but it is now close to G1494 as well, rather than the ring II 3 amino-G1494 N7 hydrogen bond observed in the prokaryotic RNA-paromomycin complex. This change also allows the 6 hydroxyl group to contact U1406; these two atoms were moderately close (4.2 Å) in the prokaryotic RNA-paromomycin complex.

The hydrogen bond from the ring III hydroxyl to G1408 might be critical in allowing paromomycin to bind to this eukaryotic sequence; this contact probably causes ring III to switch to a C2′-*endo* sugar pucker, as the hydroxyl group would be further away from the G1408 carbonyl group in a C3′-*endo* sugar pucker. No contact was observed to A1408 in the prokaryotic complex, so the contact to G1408 probably compensates for lost interactions elsewhere.

The paromomycin structure is likely stabilized by an intramolecular hydrogen bond from the ring I 2′ amino group to the ring III O4″. This contact was observed in the prokaryotic RNA-paromomycin complex. This hydrogen bond gives the first three rings of the drug a compact structure, which probably helps it fit into the RNA pocket.

Additional contacts, primarily to the phosphodiester backbone, were observed in the majority of the ensemble of 28 structures. These contacts include the ring IV 6‴ amino group to the phosphate oxygen atom of U1490 and the ring III 5″ hydroxyl group to either the phosphate oxygen atom of G1491 or N7 of G1491. Other possible contacts to the backbone observed in the ensemble of

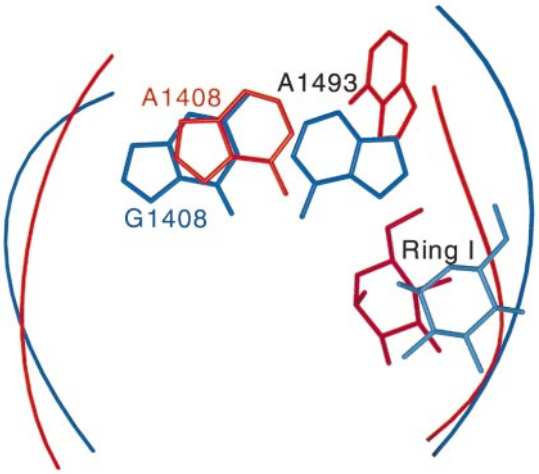

Figure 9. A top view of the superposition of the lower stem residues of the prokaryotic RNA/paromomycin complex (RNA, red; paromomycin, gold) on those of the eukaryotic RNA/paromomycin (RNA, blue; paromomycin, gold) complex. This Figure highlights the difference in position and orientation of A1493 and A/G1408. The approximate position of ring I is shown. The binding site for ring I of paromomycin is formed by the A-A base-pair, the displacement of A1492 and A1493, and the cross-strand A1408-G1494 stack.

Table 4. Specific intermolecular and intramolecular contacts of paromomycin in the eukaryotic oligonucleotide/paromomyicn complex

RNA/paromomycin atom	Paromomycin atom	Heavy atom-heavy atom distance (Å)
Ring I 2′ NH_2	Ring III 04″	2.89 ± 0.13
A1492 O (P)	Ring I 3′ OH	4.10 ± 0.77
A1493 O (P)	Ring I 6′ OH	3.32 ± 0.52
G1494 N7	Ring II 1 NH_2	2.91 ± 0.19
U1495 O4	Ring II 1 NH_2	2.91 ± 0.11
U1406 O4	Ring II 6 OH	2.69 ± 0.09
G1408 O6	Ring III 2″ OH	2.94 ± 0.27
U1406 O (P)		3.51 ± 0.77
or	Ring III 4″ OH	
C1407 O (P)		4.03 ± 0.91
G1491 O (P)		3.56 ± 0.75
or	Ring III 5″ OH	
G1491 N7		3.67 ± 0.75
U1406 O (P)	Ring IV 2‴ NH_2	4.58 ± 0.95
U1490 O (P)	Ring IV 6‴ NH_2	3.51 ± 0.95

structures include the 2‴ amino group to the phosphate oxygen atom of U1406 and the 4″ hydroxyl group to either the phosphate oxygen atom of U1406 or the phosphate oxygen atom of C1407.

Rings III and IV are disordered in both the eukaryotic and prokaryotic RNA-paromomycin complexes; thus, contacts between the RNA and paromomycin are more difficult to identify. The ring IV 6‴ amino group to U1490 contact is not the same as that observed in the prokaryotic RNA-paromomycin complex, in which the ring IV 2‴ amino group contacts the U1490 phosphate oxygen atom. The ring III 5″ hydroxyl group hydrogen bonds to N7 of G1491 in the prokaryotic RNA-paromomycin complex, but is close to either N7 or the phosphate oxygen atom of G1491 in the eukaryotic structure. Rotation around the ring III C4″-C5″ bond could put the hydrogen-bond donor close to either functional group in the eukaryotic RNA-paromomycin structure. Similar contacts were observed in the prokaryotic RNA-paromomycin complex at U1406 and C1407. Presumably, the change in sugar pucker of ring III and a slight change in orientation of ring IV to ring III in the two complexes causes the observed differences in the non-specific contacts of ring IV.

Comparison of free form and paromomycin-bound structures of the eukaryotic decoding-site oligonucleotide

Paromomycin induces a minor conformational change in the eukaryotic RNA oligonucleotide upon binding. A comparison of the free and bound forms of the eukaryotic A-site oligonucleotide is shown in Figure 13. Globally, the structures are similar, with similar internal loop base-pairs. Paromomycin induces an approximately 1.7 Å shift of the base of A1492 and a 1.3 Å shift on the base of A1493 when superimposing the lower stems of the two structures (Figure 13(a)). A1492 is shifted with respect to G1491. A1493 is shifted toward the minor groove as in the prokaryotic complex, but the shift is not as dramatic and the base does not change orientation with respect to the helix. The larger conformational changes of A1492 and A1493 in the prokaryotic complex and the small changes observed for the two bases in the eukaryotic complex are supported by dipolar coupling data (Lynch & Puglisi, 2000). An approximately 45° change of the base of G1494 relative to the base of A1493 is also observed upon binding paromomycin, determined by superimposing the base of A1493 for the two structures and measuring the angle between the two bases.

The position and orientation of G1408 relative to A1493 is affected by paromomycin binding (Figure 13(b)). Paromomycin induces an approximately 4.5 Å shift of the base of G1408 toward the lower stem and minor groove upon binding, determined by superimposing the lower stems of the two structures. In the paromomycin-bound form, G1408 is across the helix from A1493, and toward the lower stem; in the free form, G1408 is across the helix from A1493, and toward the upper stem. There is a small change of the geometry of the G-A pair. A normal G-A imino base-pair is observed in the bound structure; in contrast, a base-pair involving the guanosine amino group and A1493 N1 is observed in the free form. The drug displaces the base toward the minor groove, enabling the normal G-A imino pair. However, the shift of G1408 is not sufficient to allow formation of the binding site for ring I, because A1493 has not shifted much.

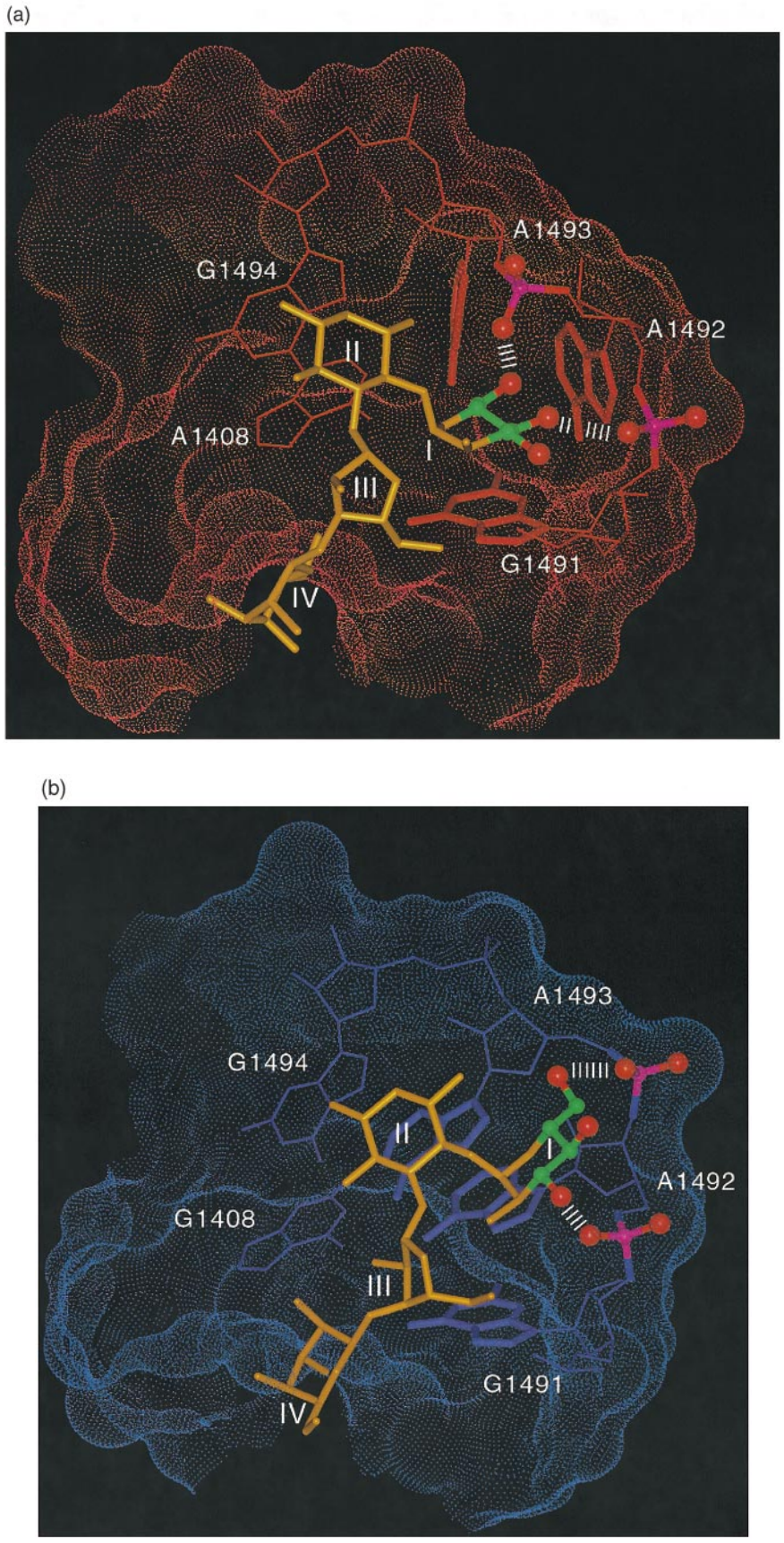

Figure 10. A comparison of the RNA surface of the prokaryotic (red) and eukaryotic (blue) structures. The position of ring I and the contacts to the RNA by paromomycin (gold) are highlighted by showing the atoms as ball and stick in their designated atomic color (red, oxygen; blue, nitrogen; pink, phosphorus). Hydrogen bonds are highlighted with broken lines.

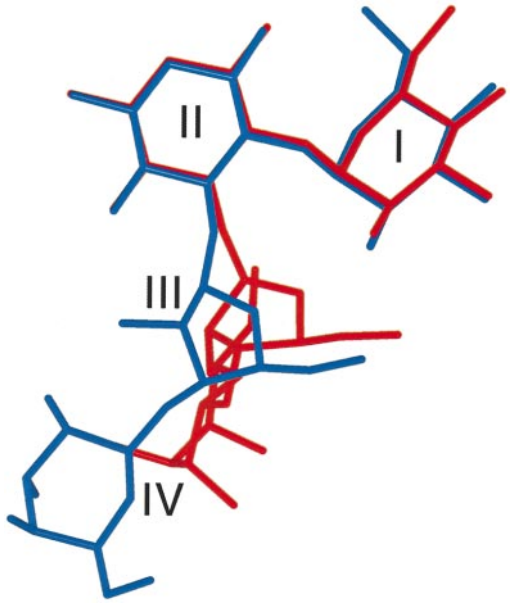

Figure 11. A superposition of the paromomycin rings I and II in the prokaryotic (red) and eukaryotic (blue) RNA/paromomycin complexes. Rings I and II adopt identical structures in the complexes; ring IV is disordered in both structures; ring III is C3′-*endo* in the prokaryotic RNA/paromomycin complex, but C2′-*endo* in the eukaryotic RNA/paromomycin complex.

Comparison of the eukaryotic RNA-paromomycin structure to chemical modification data

The eukaryotic RNA-paromomycin complex structure is consistent with previously obtained chemical modification data. Chemical modification data were published for the binding of paromomycin to the prokaryotic RNA oligonucleotide (Recht *et al*., 1996) and the ribosome (Moazed & Noller, 1987; Recht *et al*., 1996), and compared to binding of paromomycin to the A1408G mutant ribosome and eukaryotic oligonucleotide (Recht *et al*., 1999a). In both sequences, paromomycin protects G1494 from modification by dimethylsulfate (DMS), which correlates well with the structure, since paromomycin binds in the major groove and N7 of G1494 is protected by the drug. For the eukaryotic RNA oligonucleotide, a weak footprint was also observed for G1494 from kethoxal, which modifies the Watson-Crick face of guanosine nucleotides. The C1407-G1494 base-pair is observed in both the free and drug-bound RNA.

A1492 is less reactive to DMS in the eukaryotic RNA in comparison with the prokaryotic RNA. The structures support these data, because A1492 is stacked in the helix in the mutant, and less exposed to solvent. A1493 is less reactive to DMS than A1492 in the mutant, which agrees with the G1408-A1493 base-pair rather than a G1408-A1492 base-pair. The reactivity of A1493 to DMS is comparable in the prokaryotic and eukaryotic RNA oligonucleotides and is not affected by paromomycin binding. N1 of A1493 is exposed to solvent in the eukaryotic-paromomycin complex as well as in the eukaryotic RNA free form and is hydrogen bonded in both structures; the structures fit the biochemical data because paromomycin does not affect modification of A1493. The modification of A1493 is weak in comparison to G1494 and A1492, which fits with N1 of A1493 being solvent-exposed but hydrogen bonded to G1408.

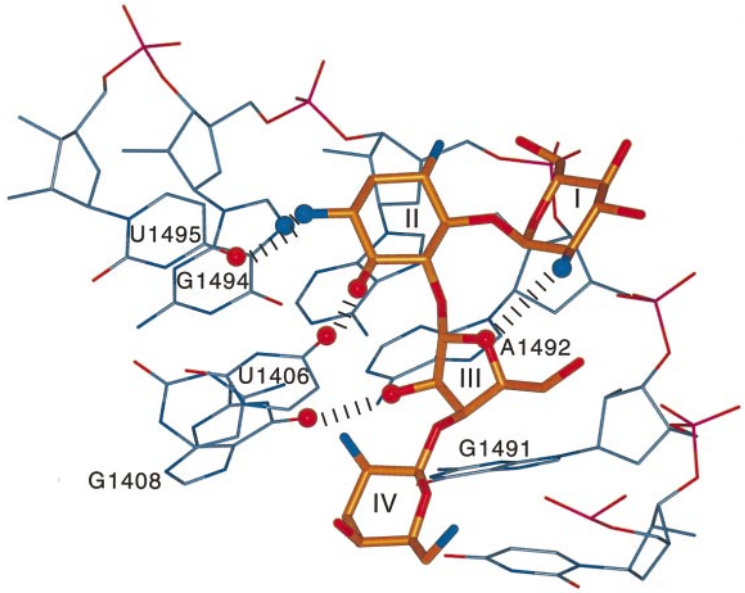

Figure 12. This Figure highlights specific contacts made by paromomycin (gold) to the eukaryotic decoding-site oligonucleotide (light blue). Hydrogen bonds are drawn as broken lines between balls with the standard atomic color scheme (red, oxygen; blue, nitrogen; pink, phosphorus).

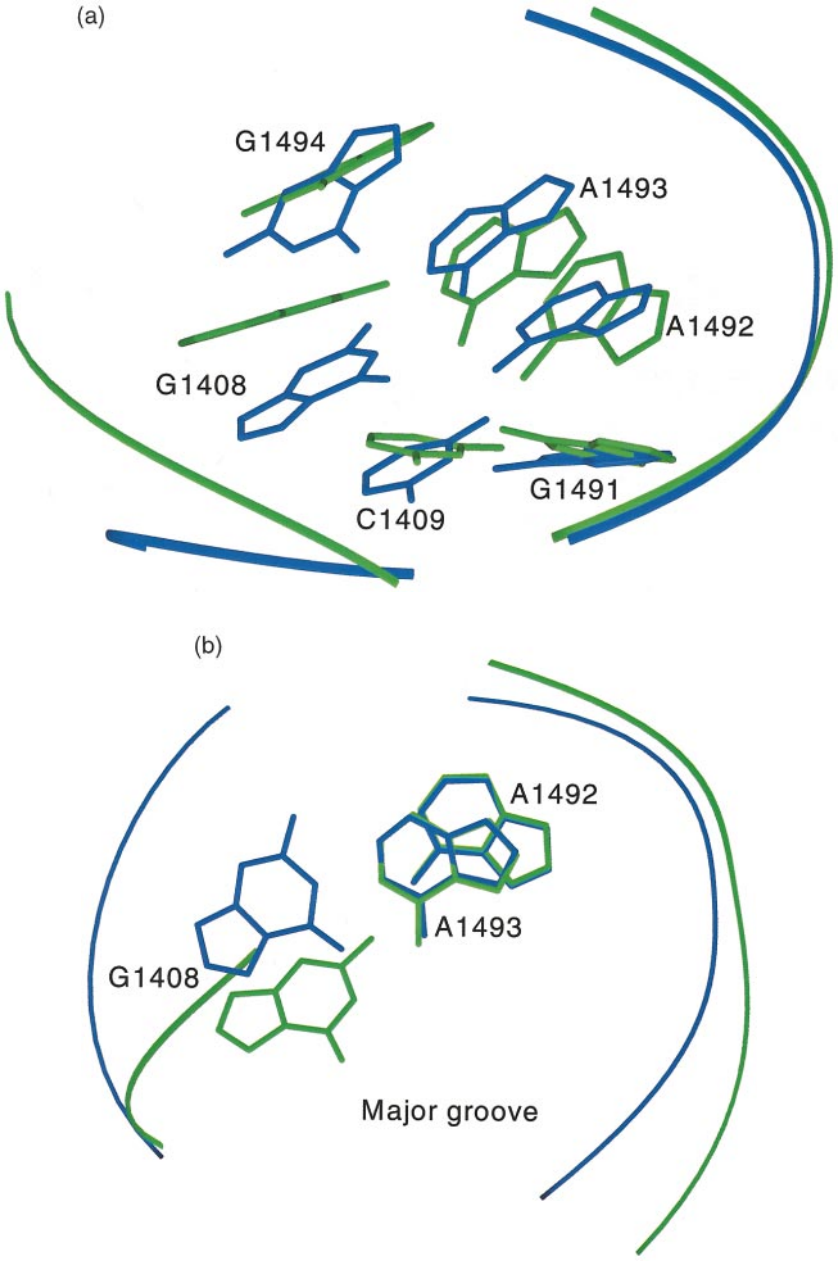

Figure 13. (a) Superposition of the lower stem of the free-form (green) and paromomycin-bound (RNA, blue; paromomycin, gold) eukaryotic RNA. The bases for G1491-G1494 and G1408-C1409 are shown, with ribbons representing the backbone. The view is into the major groove; paromomycin is not shown, but would be coming out of the page. Slight changes are observed for A1492, A1493, and G1494 upon paromomycin binding. (b) Superposition of the bases of A1492 and A1493 stem of the free-form and paromomycin-bound eukaryotic RNA. The bases of A1492, A1493, and G1408 are shown. The view is from the top of the helix down. G1408 is displaced upon paromomycin binding.

Neomycin binding to the eukaryotic decoding-site oligonucleotide

NMR spectra were acquired for neomycin bound to the eukaryotic oligonucleotide. As expected, the spectra were poorer in quality compared to the RNA-paromomycin spectra, since modification data suggested that neomycin binds with decreased affinity or specificity to this RNA sequence (Recht *et al.*, 1999a). Figure 14 presents a 1D titration of neomycin into the eukaryotic decoding-site oligonucleotide. Upon neomycin titration, the imino resonances for U1490 and G1491 shift as in the paromomycin complex (Figure 3). Several other imino resonances change upon binding of neomycin: that of G1497 shifts upfield, those for G1405 and g2 shift downfield, those for U1406 and U1495 broaden into multiple resonances, and that of G1494 broadens and becomes a shoulder on G1489.

The changes in U1490 and G1491 chemical shifts were observed for both complexes and are prob-

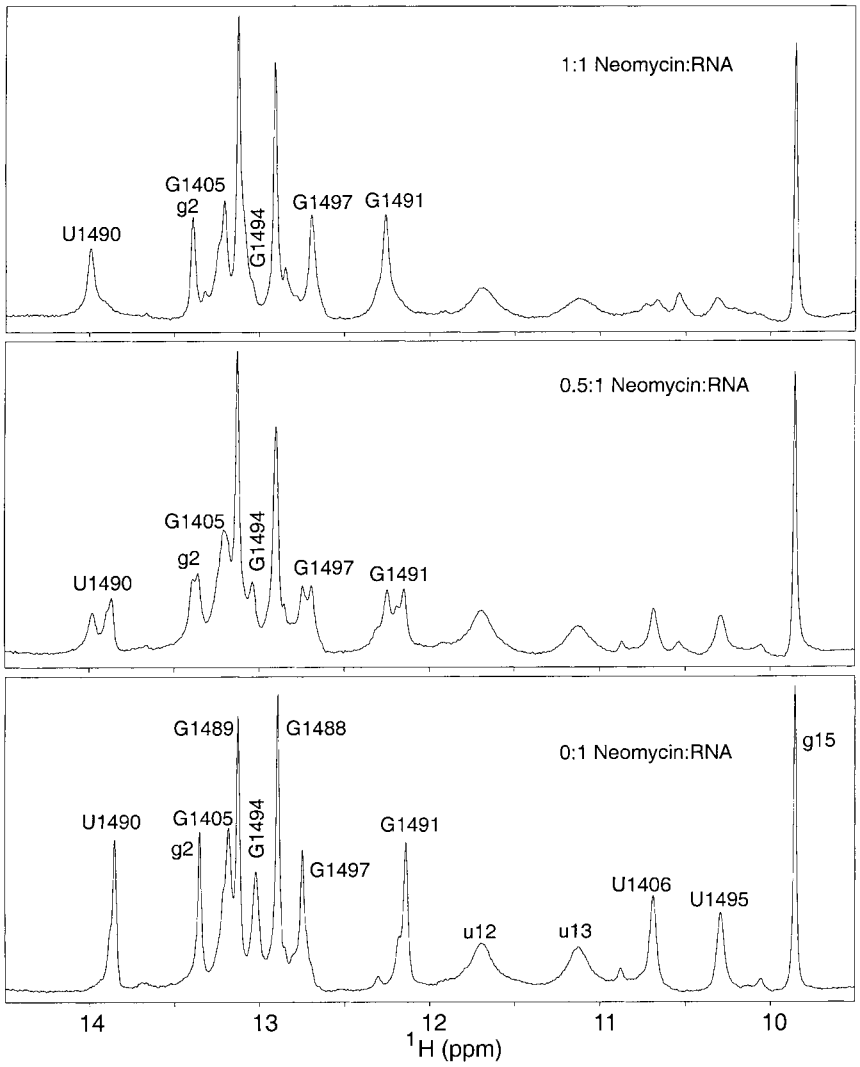

Figure 14. The 1D NMR spectrum of a titration of neomycin into the eukaryotic A-site oligonucleotide. The lower panel is the free RNA, the middle panel is a 0.5:1 complex of drug/RNA, and the top panel is a 1:1 complex. The titration was performed on a sample of 3 mM RNA at 25 °C on a Varian Inova 500 MHz spectrometer. The downfield portion of the spectrum that includes the guanosine and uridine imino proton resonances is shown. Highlighted are the protons whose resonances change upon binding of neomycin.

ably caused by binding of rings III and IV to the backbone. The changes in the chemical shifts in the upper stem resonances result from either a second binding site, multiple binding modes of a single drug, or a distortion of the closed internal loop structure that is propagated up the stem. The change in the G1494 imino resonance indicates that the Watson-Crick C1407-G1494 base-pair is either not forming or is now exchanging rapidly with solvent because it is no longer protected from solvent through stacking between A1493 and U1495. The changes in the U1406 and U1495 imino protons indicate that the two uridine nucleotides form multiple conformations. NOESY experiments in H_2O confirm that strong NOEs were observed for the multiple resonances observed between 10 ppm and 11 ppm, as expected for a U-U base-pair or, in this case, multiple conformations of U-U base-pairs.

Discussion

Aminoglycoside antibiotics specifically target prokaryotic ribosomes over eukaryotic ribosomes. In the structure of the prokaryotic oligonucleotide-paromomycin complex, the 1408 position forms a non-canonical A-A base-pair with A1493 that was previously shown to be critical for high-affinity aminoglycoside binding (Fourmy *et al.*, 1996). The 1408 position is occupied by adenosine in all prokaryotic and mitochondrial ribosomal sequences, and by guanosine in all eukaryotic cytosolic sequences. An A1408G mutation in *E. coli* confers high-level resistance to aminoglycosides with an amino group on the 6′ position of ring I, including neomycin, but only low-level resistance to aminoglycosides with a hydroxyl group at that position, including paromomycin (Recht *et al.*, 1999b). These

data correlate well with data showing A1408G resistance mutations to kanamycin, with a 6′ amino group, in *Mycobacterium* (Alangaden *et al*., 1998; Prammananan *et al*., 1998), and sensitivity of the eukaryotic organisms *Tetrahymena thermophila* and *Giardia lamblia* to aminoglycosides with a 6′ hydroxyl group (Edlind, 1989; Palmer & Wilhelm, 1978). Although A1408G ribosomes are sensitive to paromomycin, binding is decreased approximately 40-fold (Recht *et al*., 1999a). The results presented in this study show a normal G1408-A1493 imino base-pair that interferes with the binding site of ring I of paromomycin, decreasing the affinity of the drug for the eukaryotic RNA. Ring I of paromomycin makes sufficient contacts to the RNA to allow the other three rings, particularly the critical ring II, to interact specifically with the RNA. Presumably, neomycin, with the 6′ amino group on ring I, cannot make these contacts, and binds non-specifically to the RNA.

The structure of the eukaryotic decoding-site oligonucleotide-paromomycin complex is similar to prokaryotic decoding-site oligonucleotide-paromomycin complex except in the region of the A/G 1408-A1493 base-pair and the bulged A1492. Since no direct contact from paromomycin was observed to A1408 in the prokaryotic complex, the 40-fold difference in binding affinity likely results from indirect effects of position G1408. These effects most likely result from the observed change in the geometry of the purine-purine pair at the 1408-1493 positions. G1408 changes the position and orientation of A1493, which is transmitted to A1492 and G1494.

The prokaryotic RNA oligonucleotide undergoes a larger conformational change upon paromomycin binding than the eukaryotic RNA oligonucleotide. The prokaryotic RNA conformational change is possible because the Watson-Crick face of A1493 is not necessary for the A-A base-pair; N7 of A1493 hydrogen bonds to the amino group of A1408, and the six-membered ring with the bulky 6 amino group of A1493 is rotated toward the minor groove, and does not interfere with paromomycin binding. A1492 stacks under A1493, as stacking of adenosine residues is an energetically favorable interactions, and A1492 and A1493 are both rotated toward the minor groove. The cross-strand A1408-G1494 stack is also a favorable purine-purine stack causing the complete shift of A1492 and A1493 so that A1493 is base-paired but A1408 is stacked under G1494, bulging A1492 out of the helix. The bulged nucleotide creates a hole in the RNA structure. Paromomycin induces this conformational change of A1408, A1492 and A1493 in the prokaryotic complex, enabling ring I to stack on the base of G1491 in the hole created. The position of ring I directs ring II to the U1406-U1495 base-pair, and rings III and IV contact the RNA backbone to stabilize the interaction further.

The conformational change is not favorable in the eukaryotic RNA because of the geometry of the G1408-A1493 base-pair. The two common G-A base-pair geometries present bulky substituents in the major groove, which would interfere with binding of the drug. The favored base-pair for this RNA is the normal G-A imino pair (Figure 7). For the drug to induce the same conformational change on the eukaryotic RNA, either the G-A base-pair would have to be broken or the purine-purine stacking interactions would have to be disrupted.

For paromomycin to act as a drug on the ribosome, the binding of the conserved rings I and II is critical. The lack of the conformational change of A1492 and A1493 disrupts the ring I binding site. Ring I is mostly disengaged from the eukaryotic RNA, making only a few interactions to position ring II to make critical contacts to G1494 and the U1406-U1495 base-pair, which enables rings III and IV to contact the phosphodiester backbone. This result agrees with the footprinting (Recht *et al*., 1999a) and titration calorimetry data (R.G. Eason, M.I. Recht & J.D.P., unpublished results) that showed that paromomycin binds 25-50-fold weaker to the eukaryotic RNA oligonucleotide compared with the prokaryotic RNA. Although the binding is weaker, *E. coli* with the A1408G mutation is sensitive to paromomycin.

The A1408G mutation in *E. coli* confers high-level resistance to aminoglycosides with a 6′ NH_2 group, whereas only low-level resistance was observed to aminoglycosides with a 6′ OH group (Recht *et al*., 1999b). The effectiveness of aminoglycosides against *E. coli* ribosomes with an A1408G mutation mirrors the observed activities *in vitro* and *in vivo* against eukaryotic targets (Edlind, 1989; Palmer & Wilhelm, 1978; Wilhelm *et al*., 1978a,b). Thus, structural studies of the eukaryotic RNA oligonucleotide provide insights into aminoglycoside action against eukaryotic ribosomes. The preference of paromomycin (6′ OH) *versus* neomycin (6′ NH_2) for the eukaryotic oligonucleotide was revealed by NMR. Paromomycin forms a specific 1:1 complex with the oligonucleotide. In contrast, neomycin forms multiple non-specific complexes with the oligonucleotide. Evidently, neomycin, with a bulky 6′ NH_2, which is likely protonated, cannot be accommodated in the disrupted ring I binding site in the eukaryotic RNA oligonucleotide.

Aminoglycosides with either 6′ substituent bind equivalently to, and have similar activity against, prokaryotic ribosomes. The 6′ OH of paromomycin in the prokaryotic complex hydrogen bonds to the phosphate oxygen atom of A1493; the 6′ NH_2 of gentamicin C1a forms a similar interaction. In the eukaryotic complex, the 6′ OH of paromomycin can form a hydrogen bond with the phosphate oxygen atom of A1493, albeit in a much flatter RNA-binding pocket. Unfortunately, ring I is disordered in the ensemble of structures and the backbone structure in this region is poorly defined by the NMR data. A protonated amino group is slightly larger than a hydroxyl group, and the orientation of the hydrogen atoms is different. The charge difference between the 6′ OH and the 6′

NH_3^+ is not the origin for the difference in sensitivity of *E. coli* ribosomes with an A1408G mutation, as derivatives of neomycin that are neutral at the 6′ position are ineffective against the A1408G mutant ribosomes (R.G. Eason, M.I. Recht & J.D.P., unpublished results). The lack of the conformational change in the eukaryotic RNA upon paromomycin binding suggests a less flexible and more sterically constrained binding pocket for ring I, in which a 6′ NH_2 group does not fit. The binding pocket for aminoglycosides may be further constrained in the context of the 70 S particle, as this region makes intra-subunit (Clemons *et al.*, 1999) and inter-subunit contacts (Cate *et al.*, 1999). Thus, the differences observed with the oligonucleotide may be enhanced by the ribosome.

Paromomycin binds more weakly to *E. coli* ribosomes with an A1408G mutation than to wild-type *E. coli* ribosomes. The smaller decrease in activity of paromomycin against the mutant arises from the high (1-10 μM) concentration of the ribosomal target, and the 10-100 nM K_D of the drugs to the ribosome. The human cytoplasmic ribosomal target has additional mispairs in the lower stem, which disrupt the bottom of the ring I binding pocket, and would further decrease the affinity of most aminoglycosides for the target. Paromomycin works as a drug against *E. coli* ribosomes with an A1408G mutation even though the precise conformational changes of A1492 and A1493 observed in the prokaryotic-drug complexes were not observed. Nonetheless, drug binding fixes the conformation of these nucleotides with respect to the unbound form. Small local conformational changes in this region of ribosomal RNA are likely critical for ribosome function in initiation, elongation and decoding, and termination. Conformational signals may be transmitted from the decoding-site to the 50 S subunit through the 900 region and the penultimate stem. Aminoglycoside binding to either the wild-type or mutant G1408 ribosomes probably shifts the subtle conformational equilibria required for this signaling, thus inhibiting translation.

To understand aminoglycoside activity and toxicity further, the structures of the drugs bound to the bacterial and human targets are needed. The structure of the eukaryotic RNA-paromomycin complex provides insights into aminoglycoside binding to eukaryotic ribosomal RNA. This allows a structural framework for designing improved specificity for these drugs. Beyond the problem of aminoglycoside toxicity, aminoglycoside activity against eukaryotic ribosomes may play a beneficial role in therapies of genetic diseases, as aminoglycosides cause readthrough of premature stop codons (Barton-Davis *et al.*, 1999; Burke & Mogg, 1985; Wilschanski *et al.*, 2000). The structure presented here provides a rationale for the design of aminoglycosides with improved activities against eukaryotic ribosomes.

Materials and Methods

NMR sample preparation

Milligram quantities of the eukaryotic decoding-site RNA oligonucleotide were prepared unlabeled and uniformly ^{13}C,^{15}N-labeled by *in vitro* transcription from an oligonucleotide template and purified as described (Puglisi & Wyatt, 1995). After electro-elution and precipitation in ethanol, the RNA pellet was resuspended in 10 mM sodium phosphate (pH 6.3), 20 μM EDTA. The sample was then dialyzed against the phosphate buffer with a stepwise decrease in sodium chloride from 1 M to 0 in a microdialysis apparatus with a 1000 Da cut-off membrane. The buffer used for most NMR experiments was 10 mM sodium phosphate (pH 6.3), 20 μM EDTA. Some H_2O NOESY experiments were acquired in pH 5.75 buffer to slow the exchange rate of imino protons. Paromomycin and neomycin were purchased from Sigma and not purified further. A 1:1 complex of RNA and paromomycin or neomycin was prepared by monitoring the chemical shift changes of imino protons. NMR samples were either 3 mM (unlabeled) or 1.8 mM (^{13}C,^{15}N-labeled) in 230 μl in a Shigemi NMR tube.

NMR spectroscopy

NMR experiments were acquired on either a Varian Inova 500 MHz or Varian Inova 800 MHz spectrometer with triple resonance and three axis gradient capabilities. NMR data were processed using either VNMR (Varian) or Felix (Molecular Simulations Incorporated, San Diego, CA) software. ^1H chemical shifts were referenced directly to trimethylsilyl propionic acid (TSP); ^{15}N and ^{13}C chemical shifts were referenced to known chemical shifts of imino nitrogen atoms and ribose carbon atoms in the UUCG tetraloop (Varani & Tinoco, 1991).

The exchangeable proton resonances of the RNA were assigned using a combination of through-space homonuclear NOESY experiments at different temperatures (5, 15 and 25 °C) and different mixing times (75 ms, 150 ms and 250 ms), and through-bond correlation experiments of exchangeable protons and non-exchangeable protons in H_2O. Water suppression for these experiments was accomplished using either a 1:1 jump-return (Otting *et al.*, 1987) or WATERGATE sequence (Piotto *et al.*, 1992).

The non-exchangeable proton resonances of the RNA were assigned with a combination of homonuclear NOESY experiments at different temperatures (15, 20, 25 and 35 °C) and different mixing times (50 ms, 100 ms, 150 ms, 250 ms and 300 ms), heteronuclear 3D (^{13}C) edited NOESY experiments (Clore *et al.*, 1990) centered on either the aromatic or ribose portions of the carbon spectrum at 35 °C for the complex with paromomycin with a mixing time of 150 ms, and heteronuclear through-bond experiments. 3D HCCH-TOCSY (Clore *et al.*, 1990; Nikonowicz & Pardi, 1992) was used to correlate protons within one spin system. 3D HCP (Marino *et al.*, 1994b) experiment and 2D $^1H/^{31}P$ heteronuclear COSY (Sklénar *et al.*, 1986) were used to connect successive nucleotides through the ^{31}P. MQ-HCN (Marino *et al.*, 1997) was used to correlate the H1′ and H8/H6. 2D HCCH-TOCSY (Marino *et al.*, 1994a) was used to correlate the H2 and H8 resonances on the adenosine residues. The pyrimidine H5 and H6 were correlated by a DQF-COSY. Parameters for the DQF-COSY were 4096 complex points in ω2, 512 complex points in ω1, with 32 scans/increment with a relaxation delay of 1.5 seconds Heteronuclear TOCSY experiments were used to correlate the water-

exchangeable base protons with the non-exchangeable protons on the base (Simorre *et al*., 1995, 1996a,b).

The non-exchangeable resonances of paromomycin were assigned with through-bond experiments exclusively. The resonances within each ring were correlated by homonuclear TOCSY with a mixing time of 80 ms. The sequential assignment was then accomplished by correlating the protons two and three bonds apart with either DQF-COSY or TOCSY at 20 ms. The $^{13}C/^{1}H$ HMQC in natural abundance was used to separate antibiotic protons by type.

Structure calculation

Structures of the RNA oligonucleotide-drug complexes were calculated using restrained molecular dynamics followed by energy minimization using the program X-PLOR on an SGI Octane workstation with a force-field consisting of bond lengths, bond angles, improper angles, repulsive van der Waals potentials, and experimental distance and dihedral constraints in the absence of electrostatics. Random starting structures for the RNA were created by randomizing torsion angles for the calculation. Paromomycin was initially started 20 Å from the RNA and allowed to fold simultaneously with the RNA. The initial stage was a modified simulated annealing protocol (Wimberly *et al*., 1993) that included experimental distance constraints but did not include dihedral constraints; structures that converged to low total energy were subjected to a refinement protocol that added in the experimental dihedral constraints. Of 100 structures, 35 initially converged in the paromomycin complex. The structures were finally minimized with attractive Lennard-Jones potentials to obtain ideal van der Waals contacts. The final structures were displayed with the program Insight II (Molecular Simulations Incorporated, San Diego, CA). The energy of seven final structures diverged after addition of torsion angle constraints and either violated an NOE or dihedral constraint. These structures were discounted.

Distance restraints were assigned on the basis of NOE volumes of crosspeaks in NOESY experiments at short mixing time (50 ms), medium mixing time (100 ms), and long mixing time (150 ms). NOEs with volumes comparable to those of the H1′-H2′ and pyrimidine H5-H6 NOEs at short mixing time were assigned as strong and given a distance range of 1.8-3.0 Å. NOEs that were weaker than the strong NOEs at short mixing time but were intense at medium mixing time were assigned as medium and given a distance range of 2-4.5 Å. NOEs that were not intense until long mixing time were assigned as weak and given a distance range of 3-6 Å. NOEs that were weak in intensity at 150 ms were assigned as very weak and given a range of 3.5-7.5 Å. NOEs that were clearly identifiable but whose intensity was hard to define due to overlap were given wider ranges depending on the mixing time. Water-exchangeable NOEs were assigned wide ranges on the basis of their intensity in a 75 ms mixing time NOESY in H_2O. Since intermolecular NOEs between the RNA and the antibiotic were always weaker in intensity than the intramolecular NOEs, the distance ranges assigned were wide and based upon what mixing time they were first observed. NOEs observed at 100 ms were assigned as 1.8-4.5 Å. NOEs observed only at 150 ms were assigned as 2.0-6.0 Å. Finally, NOEs that were not observed until longer mixing times were assigned as 3.0-7.5 Å. Somewhat tighter constraints were initially used on the tetraloop to achieve higher convergence; the structure of the tetraloop was determined previously and is not discussed here.

Dihedral constraints were determined from homonuclear and heteronuclear correlation experiments, except for the χ angle, which was assigned on the basis of the presence or absence of a strong H1′-H8/H6 NOE. All nucleotides were assigned as *anti* except the G of the UUCG tetraloop as previously shown (Cheong *et al*., 1990). *Anti* was assigned a range of $-40°$-$180°$ (O4′-C1′-N9/N1-C4/C2) (Saenger, 1984).

The ribose sugar pucker was assigned on the basis of the value of the H1′-H2′ coupling constant determined in a DQF-COSY. A coupling constant >8 Hz was assigned as C2′-*endo*; a coupling constant < 2 Hz was assigned as C3′-*endo*. Nucleotides with coupling constants between 2 Hz and 8 Hz were assigned as mixed and given a range of sugar puckers from C2′-*endo*, O4′-*endo* and C3′-*endo*. The values for each were from Saenger (1984).

The backbone torsion angles were determined essentially as described by Marino *et al*. (1999) and by Fourmy *et al*. (1998). Overlap, particularly in phosphorus chemical shift, prevented all angles from being identified. Values for these angles were from Saenger (1984) with ranges of $\pm 20°$. The backbone torsion angle ε was estimated from $^{3}J_{H3'\text{-}P}$, $^{3}J_{C2'\text{-}P}$, and $^{3}J_{C4'\text{-}P}$ from a 2D ^{31}P-^{1}H heteronuclear COSY (Sklénar *et al*., 1986) and 3D HCP (Marino *et al*., 1994b) and given a range of $-155(\pm 20)°$, except for c14 of the UUCG loop, which was given a range of $-95(\pm 20)°$. The torsion angle β was estimated from $^{3}J_{H5'\text{-}P}$, $^{3}J_{H5''\text{-}P}$, and $^{3}J_{C4'\text{-}P}$ from the same experiments and given a range of $180(\pm 20)°$. The torsion angles β for G1408 and G1491-G1494 were not confidently assigned and not constrained. The torsion angle γ was estimated from $^{3}J_{H4'\text{-}H5'}$ from a ^{31}P decoupled DQF-COSY and a 3D ^{13}C-^{1}H HMQC-TOCSY, and given a range of $55(\pm 20)°$, except for g15 of the UUCG loop, which is *trans* and given a range of $180(\pm 20)°$. The torsion angle γ for G1408 and G1491-G1494 were not confidently assigned and not constrained.

Torsion angle constraints for paromomycin were determined by measuring possible $^{3}J_{1H1H}$ in a DQF-COSY experiment and comparing the values to the Karplus relationship of scalar coupling constant *versus* torsion angle. Constraints were used in the calculation when each $^{3}J_{1H1H}$ within the individual rings was consistent with one ring conformation. The torsion angle constraints were $\pm 20°$ from the median.

Protein Data Bank accession code

Coordinates have been deposited in the PDB RCSB protein data bank, accession number 1FYP.

Acknowledgments

We thank M. Recht, K. Dahlquist, R. G. Eason, S. Yoshizawa and S. Blanchard for many useful discussions on aminoglycosides and the ribosome, and P. Lukavsky for writing NMR pulse sequences used in these studies. This work was supported by NIH grant GM51266 and funding from Aventis Pharmaceuticals. The Stanford Magnetic Resonance Laborabory is supported by the Stanford Medical School.

References

Alangaden, G. J., Kreiswirth, B. N., Aouad, A., Khetarpal, M., Igno, F. R., Moghazeh, S. L., Manavathu, E. K. & Lerner, S. A. (1998). Mechanism of resistance to amikacin and kanamycin in *Mycobacterium tuberculosis*. *Antimicrob. Agents Chemother.* **42**, 1295-1297.

Barton-Davis, E. R., Cordier, L., Shoturma, D. I., Leland, S. E. & Sweeney, H. L. (1999). Aminoglycoside antibiotics restore dystrophin function to skeletal muscles of mdx mice. *J. Clin. Invest.* **104**, 375-381.

Burke, J. F. & Mogg, A. E. (1985). Suppression of a nonsense mutation in mammalian cells in vivo by the aminoglycoside antibiotics G-418 and paromomycin. *Nucl. Acids Res.* **13**, 6265-6272.

Cate, J. H., Yusupov, M. M., Yusupova, G. Z., Earnest, T. N. & Noller, H. F. (1999). X-ray crystal structures of 70 S ribosome functional complexes. *Science,* **285**, 2095-2104.

Cheong, C., Varani, G. & Tinoco, I., Jr (1990). Solution structure of an unusually stable RNA hairpin, 5′GGAC(UUCG)GUCC. *Nature,* **346**, 680-682.

Clemons, W. M., May, J. L., Wimberly, B. T., McCutcheon, J. P., Capel, M. S. & Ramakrishnan, V. (1999). Structure of a bacterial 30 S ribosomal subunit at 5.5 Å resolution. *Nature,* **400**, 833-840.

Clore, G. M., Bax, A., Driscoll, P. C., Wingfield, P. T. & Gronenborn, A. M. (1990). Assignment of the side-chain ^{1}H and ^{13}C resonances of interleukin-1β using double- and triple-resonance heteronuclear three-dimensional NMR spectroscopy. *Biochemistry,* **29**, 8172-8184.

Davies, J., Gorini, L. & Davis, B. D. (1965). Misreading of RNA codewords induced by aminoglycoside antibiotics. *Mol. Pharmacol.* **1**, 93-106.

Edelmann, P. & Gallant, J. (1977). Mistranslation in *E. coli*. *Cell,* **10**, 131-137.

Edlind, T. D. (1989). Susceptibility of *Giardia lamblia* to aminoglycoside protein synthesis inhibitors: correlation with rRNA structure. *Antimicrob. Agents Chemother.* **33**, 484-488.

Fourmy, D., Recht, M. I., Blanchard, S. C. & Puglisi, J. D. (1996). Structure of the A site of *E. coli* 16 S ribosomal RNA complexed with an aminoglycoside antibiotic. *Science,* **274**, 1367-1371.

Fourmy, D., Yoshizawa, S. & Puglisi, J. D. (1998). Paromomycin binding induces a local conformational change in the A site of 16 S rRNA. *J. Mol. Biol.* **277**, 333-345.

Gutell, R. R. (1994). Collection of small subunit (16 S- and 16 S-like) ribosomal RNA structures: 1994. *Nucl. Acids Res.* **22**, 3502-3507.

Lynch, S. R. & Puglisi, J. D. (2000). Application of residual dipolar coupling measurements to identify conformational changes in RNA induced by antibiotics. *J. Am. Chem. Soc.* **122**, 7853-7854.

Lynch, S. R. & Puglisi, J. D. (2001). Structure of a eukaryotic decoding region A site RNA. *J. Mol. Biol.* **306**, 1023-1035.

Marino, J. P., Prestegard, J. H. & Crothers, D. M. (1994a). Correlation of adenine H2/H8 resonances in uniformly ^{13}C labeled RNAs by 2D HCCH-TOCSY: a new tool for ^{1}H assignment. *J. Am. Chem. Soc.* **116**, 2205-2206.

Marino, J. P., Schwalbe, H., Anklin, C., Bermel, W., Crothers, D. M. & Griesinger, C. (1994b). A three-dimensional triple-resonance ^{1}H, ^{13}C, ^{31}P experiment: sequential through-bond correlation of ribose protons and intervening phosphorus along the RNA oligonucleotide backbone. *J. Am. Chem. Soc.* **116**, 6472-6473.

Marino, J. P., Diener, J. L., Moore, P. B. & Griesinger, C. (1997). Multiple-quantum coherence dramatically enhances the sensitivity of CH and CH_2 correlations in uniformly ^{13}C-labeled RNA. *J. Am Chem. Soc.* **119**, 7361-7366.

Marino, J. P., Schwalbe, H. & Griesinger, C. (1999). *J*-coupling restraints in RNA structure determination. *Accts. Chem. Res.* **32**, 614-623.

Moazed, D. & Noller, H. F. (1987). Interaction of antibiotics with functional sites in 16 S ribosomal RNA. *Nature,* **327**, 389-394.

Nikonowicz, E. P. & Pardi, A. (1992). Three-dimensional heteronuclear NMR studies of RNA. *Nature,* **355**, 184-186.

Otting, G., Grutter, R., Leupin, W., Minganti, C., Ganesh, K. N., Sproat, B. S., Gait, M. J. & Wuthrich, K. (1987). Sequential NMR assignments of labile protons in DNA using two-dimensional nuclear-Overhauser-enhancement spectroscopy with three jump-and-return pulse sequences. *Eur. J. Biochem.* **166**, 215-220.

Palmer, E. & Wilhelm, J. M. (1978). Mistranslation in a eukaryotic organism. *Cell,* **13**, 329-334.

Piotto, M., Saudek, V. & Sklenár, V. (1992). Gradient-tailored excitation for single-quantum NMR spectroscopy of aqueous solutions. *J. Biomol. NMR,* **2**, 661-665.

Prammananan, T., Sander, P., Brown, B. A., Frischkorn, K., Onyi, G. O., Zhang, Y., Bottger, E. C. & Wallace, R. J., Jr (1998). A single 16 S ribosomal RNA substitution is responsible for resistance to amikacin and other 2-deoxystreptamine aminoglycosides in *Mycobacterium abscessus* and *Mycobacterium chelonae*. *J. Infect. Dis.* **177**, 1573-1581.

Puglisi, J. D. & Wyatt, J. R. (1995). Biochemical and NMR studies of RNA conformation with an emphasis on RNA pseudoknots. *Methods Enzymol.* **261**, 323-350.

Recht, M. I., Fourmy, D., Blanchard, S. C., Dahlquist, K. D. & Puglisi, J. D. (1996). RNA sequence determinants for aminoglycoside binding to an A-site rRNA model oligonucleotide. *J. Mol. Biol.* **262**, 421-436.

Recht, M. I., Douthwaite, S., Dahlquist, K. D. & Puglisi, J. D. (1999a). Effect of mutations in the A site of 16 S rRNA on aminoglycoside antibiotic-ribosome interaction. *J. Mol. Biol.* **286**, 33-43.

Recht, M. I., Douthwaite, S. & Puglisi, J. D. (1999b). Basis for prokaryotic specificity of action of aminoglycoside antibiotics. *EMBO J.* **18**, 3133-3138.

Saenger, W. (1984). *Principles of Nucleic Acid Structure*, Springer-Verlag, Berlin.

Simorre, J.-P., Zimmermann, G. R., Pardi, A., Farmer, B. T. I. & Mueller, L. (1995). Triple resonance HNCCCH experiments for correlating exchangeable cytidine and uridine base protons in RNA. *J. Biomol. NMR,* **6**, 427-432.

Simorre, J.-P., Zimmermann, G. R., Mueller, L. & Pardi, A. (1996a). Correlations of the guanosine exchangeable and nonexchangeable base protons in ^{13}C-^{15}N-labeled RNA with an HNC-TOCSY-CH experiment. *J. Biomol. NMR,* **7**, 153-156.

Simorre, J. P., Zimmermann, G. R., Mueller, L. & Pardi, A. (1996b). Triple-resonance experiments for assignment of adenine base resonances in $^{13}C/^{15}N$ labeled RNA. *J. Am. Chem. Soc.* **118**, 5316-5317.

Sklénar, V., Miyashiro, H., Zon, G. & Bax, A. (1986). Assignment of the ^{31}P and ^{1}H resonances in oligonucleotides by two-dimensional NMR spectroscopy. *FEBS Letters,* **208**, 94-98.

Varani, G. & Tinoco, I., Jr (1991). Carbon assignments and heteronuclear coupling constants for an RNA oligonucleotide form natural abundance ^{13}C-^{1}H correlated experiments. *J. Am. Chem. Soc.* **113**, 9349-9354.

Wilhelm, J. M., Pettitt, S. E. & Jessop, J. J. (1978a). Aminoglycoside antibiotics and eukaryotic protein synthesis: structure-function relationships in the stimulation of misreading with a wheat embryo system. *Biochemistry,* **17**, 1143-1149.

Wilhelm, J. M., Jessop, J. J. & Pettitt, S. E. (1978b). Aminoglycoside antibiotics and eukaryotic protein synthesis: stimulation of errors in the translation of natural messengers in extracts of cultured human cells. *Biochemistry,* **17**, 1149-1153.

Wilschanski, M., Famini, C., Blau, H., Rivlin, J., Augarten, A., Avital, A., Kerem, B. & Kerem, E. (2000). A pilot study of the effect of gentamicin on nasal potential difference measurements in cystic fibrosis patients carrying stop mutations. *Am. J. Respir. Crit. Care Med.* **161**, 860-865.

Wimberly, B., Varani, G. & Tinoco, I., Jr (1993). The conformation of loop E of eukaryotic 5S ribosomal RNA. *Biochemistry,* **32**, 1078-1087.

Woodcock, J., Moazed, D., Cannon, M., Davies, J. & Noller, H. F. (1991). Interaction of antibiotics with A- and P-site-specific bases in 16 S ribosomal RNA. *EMBO J.* **10**, 3099-3103.

Yoshizawa, S., Fourmy, D. & Puglisi, J. D. (1998). Structural origins of gentamicin antibiotic action. *EMBO J.* **17**, 6437-6448.

Edited by I. Tinoco

(Received 11 July 2000; received in revised form 10 October 2000; accepted 20 December 2000)

http://www.academicpress.com/jmb

Supplementary Material is available on IDEAL